Science Advances
AAAS

advances.sciencemag.org/cgi/content/full/5/2/eaau2124/DC1

Supplementary Materials for

Nano-bio-computing lipid nanotablet

Jinyoung Seo, Sungi Kim, Ha H. Park, Da Yeon Choi, Jwa-Min Nam*

*Corresponding author. Email: jmnam@snu.ac.kr

Published 22 February 2019, *Sci. Adv.* **5**, eaau2124 (2019)
DOI: 10.1126/sciadv.aau2124

The PDF file includes:

Other Supplementary Material for this manuscript includes the following:

(available at advances.sciencemag.org/cgi/content/full/5/2/eaau2124/DC1)

Movie S1 (.mp4 format). Time-lapse dark-field imaging of a nanoparticle Assembly YES gate.
Movie S2 (.mp4 format). Time-lapse dark-field imaging of a nanoparticle Disassembly YES gate.
Movie S3 (.mp4 format). Receptor-only visualization of a dark-field movie.
Movie S4 (.mp4 format). Time-lapse dark-field imaging of a two-input Assembly AND gate.
Movie S5 (.mp4 format). Time-lapse dark-field imaging of a two-input Assembly OR gate.
Movie S6 (.mp4 format). Time-lapse dark-field imaging of a two-input Disassembly AND gate.
Movie S7 (.mp4 format). Time-lapse dark-field imaging of a two-input Disassembly OR gate.
Movie S8 (.mp4 format). Time-lapse dark-field imaging of a two-input Disassembly INHIBIT gate.
Movie S9 (.mp4 format). Time-lapse dark-field imaging of a six-input Disassembly gate.
Movie S10 (.mp4 format). Time-lapse dark-field imaging of a two-input Disassembly AND gate with three outputs.
Movie S11 (.mp4 format). Time-lapse dark-field imaging of a two-layer AND-AND cascade circuit.
Movie S12 (.mp4 format). Time-lapse dark-field imaging of a two-layer AND-OR cascade circuit.
Movie S13 (.mp4 format). Time-lapse dark-field imaging of a nanoparticle multiplexer circuit.

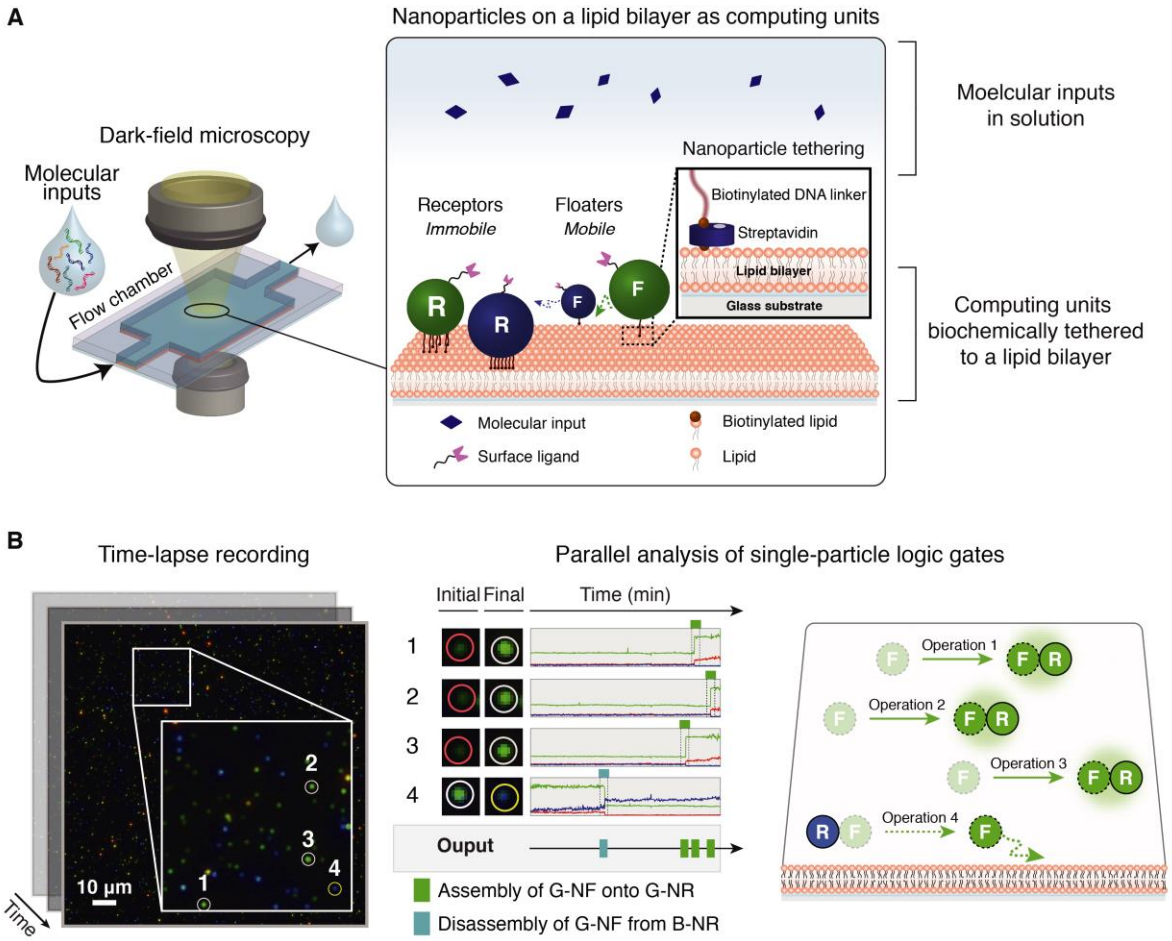

Fig. S1. Conceptual illustrations of the LNT platform. A lipid nanotablet (LNT) takes molecules as inputs and performs nanoparticle logic computation via nanoparticle networks tethered to its supported lipid bilayer, inducing dynamic assembly/disassembly reactions of nanoparticles as outputs. The plasmonic nanoparticles act as computing units and provide *in situ* optical readout as outputs that are readily readable and analyzable by dark-field microscopy (DFM). (**A**) Supported lipid bilayers as chemical circuit boards for nanoparticle computation. In LNT platform, the nanoparticle logic units are tethered to the lipid bilayer surface via strong interaction between biotinylated DNA linkers on the nanoparticle surfaces and streptavidins bound to biotinylated lipid molecules. On a lipid bilayer, receptor nanoparticles (R) are immobile due to a large number of surface DNA linkers that strongly interact with the lipid surface, and floater nanoparticles (F) are freely diffusible due to low linker density. Depending on the scattering signals of core nanoparticles, receptors are referred to as red nano-receptors (R-NRs), green nano-receptors (G-NRs), or blue nano-receptors (B-NRs). Similarly, floaters are referred to as red nano-floaters (R-NRs), green nano-floaters (G-NFs) or blue nano-floaters (B-NFs). Receptors and floaters serve as logic gates, processing the molecular information in solution using their programmable, stimuli-responsive surface ligands. Once nanoparticle logic gates are integrated on the lipid bilayer "chip", solutions such as wash buffer and those containing nanoparticle gates or molecular inputs can be exchanged without perturbing the tethered particles. In addition, the dark-field imaging can be performed during the solution exchange *in situ*. (**B**) Parallel, single-particle analysis of nanoparticles by DFM. On LNT platform, multiple nanoparticle logic gates can be analyzed in parallel as long as each logic gate generates a spectrally distinct optical signal as an output. Several logic gates can be readily designed to generate distinct optical signals because plasmonic coupling-induced changes in a nanoparticle scattering signal depend on the combinations of receptor–floater pair involved in the interaction (*36*). A simple example of parallel, single-particle analysis on LNTs is illustrated. In this example, an Assembly logic gate is composed of a G-NR and a G-NF, and a Disassembly logic gate is composed of a B-NR and a G-NF. The two output signals of the two logic gates, an increase in green intensity of a G-NR (by association with a G-NF) and a decrease in the green intensity of a B-NR (by dissociation with a G-NF), are readily discernible. Thus, the two gates can be executed simultaneously.

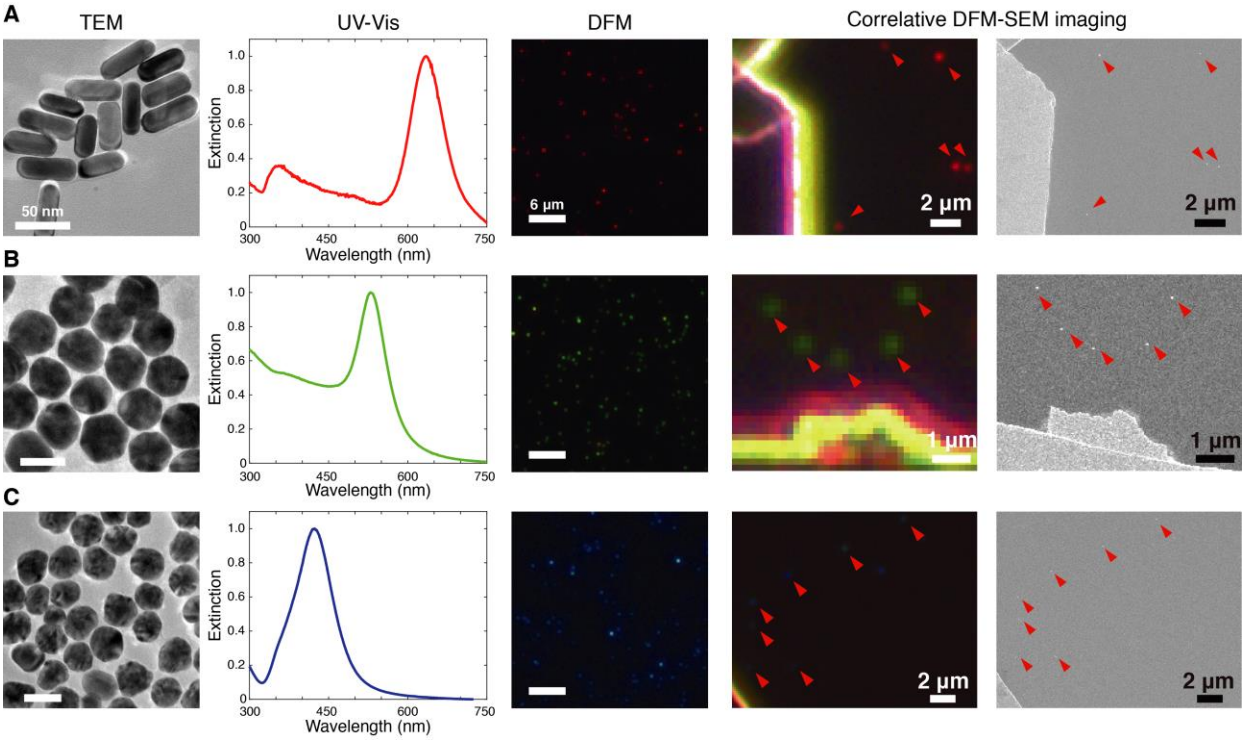

Fig. S2. Characterization of nanoparticles. (**A**) Gold nanorods with silver shells (diameter = 22.2 ± 1.2 nm, length = 55.9 ± 2.9 nm, aspect ratio = 2.5) that serve as core red nanoparticles for R-NRs and R-NFs. (**B**) Gold nanospheres (diameters = 50.0 ± 1.8 nm) used as core green particles for G-NRs and G-NFs. (**C**) Silver nanospheres with gold seeds (diameters = 54.8 ± 3.1 nm) that function as core blue particles for B-NRs and B-NFs. First column: transmission electron microscopy images. Second column: extinction spectra obtained by an ultraviolet–visible spectrophotometer. The three spectra were normalized to 1 OD. Third column: DFM images of nanoparticles tethered to a supported lipid bilayer. Fourth and fifth columns: Correlative DFM-SEM imaging for single-nanoparticle scattering signal analysis. Nanoparticles on a Cr-patterned glass substrate were first imaged by DFM, coated with Pt, and imaged in the same position by FE-SEM. As nanoparticles exhibit plasmonic coupling effect when the two nanoparticles are located in a close distance, we could determine whether a bright spot is from a single particle or an aggregation. The SEM images taken in the same positions (right) show that bright spots captured in the DFM images (left) are from single nanoparticles.

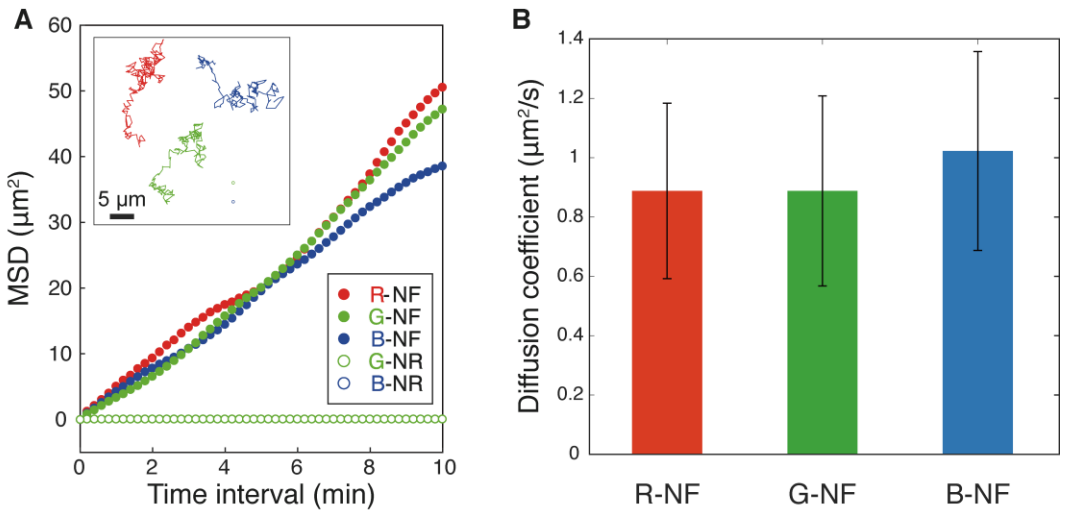

Fig. S3. Diffusion of nanoparticles tethered to an SLB. (**A**) Mean square displacement (MSD) versus time plots of the five representative diffusion trajectories (inset). The MSD plots of the three mobile floaters, R-NFs, G-NFs, and B-NFs, showed a linear relationship that confirmed their two-dimensional Brownian motions. The MSD plots of G-NRs and B-NRs confirmed their immobility. (**B**) Average diffusion coefficients of the diffusive R-NF (N = 154), G-NF (N = 194), and B-NFs (N = 247). Error bars indicate standard deviations.

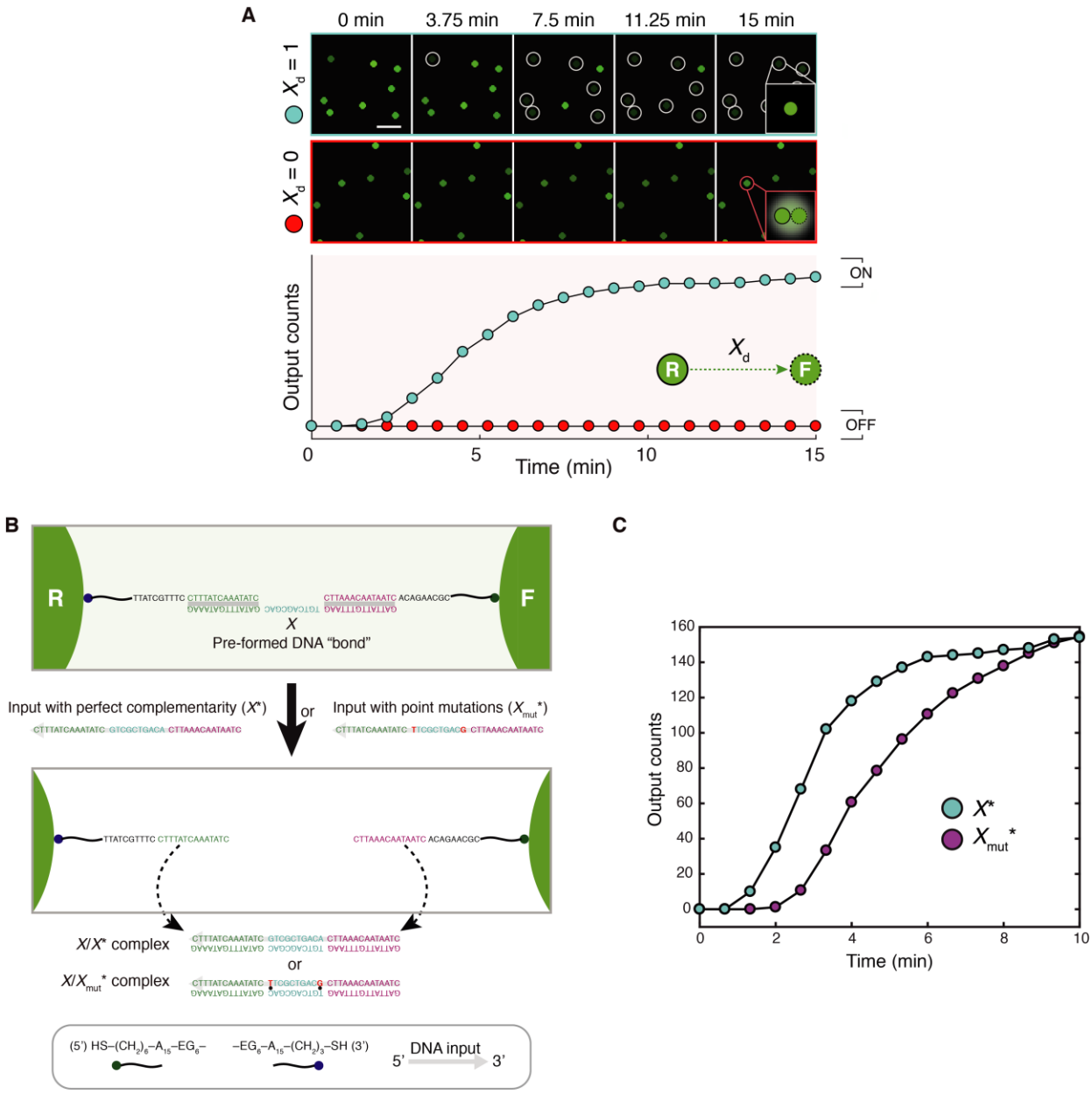

Fig. S4. Design and implementation of a Disassembly YES gate. (**A**) DNA-mediated disassembly reactions captured by DFM imaging. Inputs were added after pre-dimerization. G-NFs are released from G-NRs only when a disassembly input X_d (in Fig. 1C) is present in solution. The disassembly events were cumulatively counted as outputs of the Disassembly YES gate. The time-versus-output plot indicates that the population of Disassembly YES gate switches into ON state in response to X_d. (**B**) Nucleotide-level illustrations of a Disassembly YES gate responding to a fully complementary input (X*) and a mismatched input (X_{mut}*). Two point mutations at both ends of the toehold domain (A to G, G to T) and mismatched base pairings are highlighted. (**C**) Kinetics analysis. Fully complementary and mismatched inputs are shown in cyan and magenta, respectively. Due to the high concentration (500 nM) of input and long toehold domain, equilibrium is pushed toward disassembly even in the presence of base mismatches. As a result, responses under both conditions were saturated after sufficient operation time. However, the fully complementary input induced faster response of the disassembly gate than the mismatched input, which indicated that the system could potentially discriminate mismatched inputs under certain conditions. EG denotes an ethylene glycol unit. Asterisks denote complementarity.

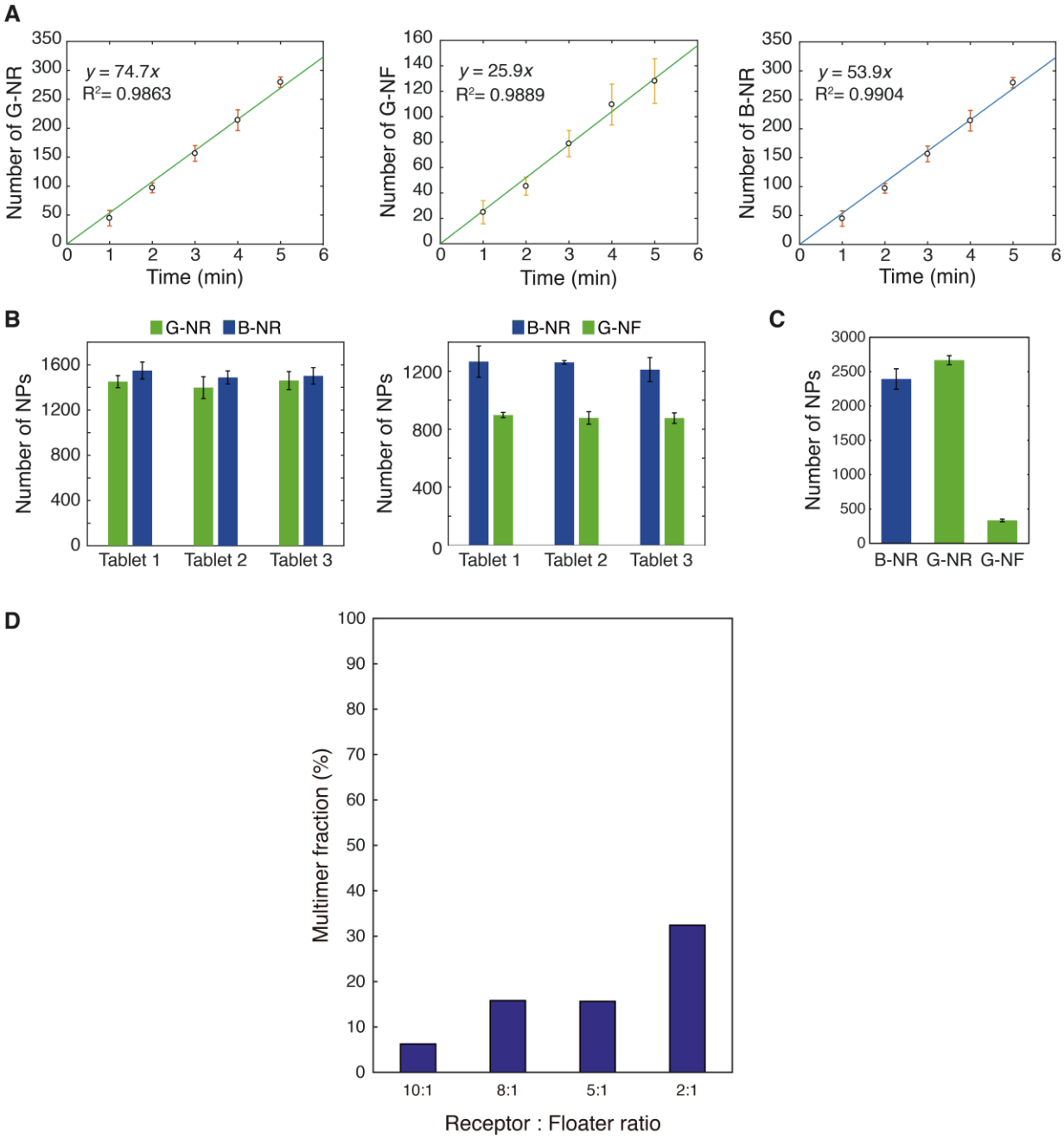

Fig. S5. Tethering of nanoparticles to an SLB. (**A**) The number of nanoparticles (NPs) tethered to a supported lipid bilayer versus incubation time plots. Tethering of 2.5 pM G-NR (left), 2.6 pM G-NF (center) and 2.2 pM B-NR (right). The number of NPs at each time point was counted in an area of 90 × 90 μm^2 at four different positions. Error bars indicate standard deviations calculated based on the particle numbers counted at the four positions. The plots showed that the number of tethered particles is linearly proportional to the time during which a lipid bilayer chambers is incubated with the solution containing biotinylated NPs ($R^2 > 0.98$). The plots also revealed that tethering of receptors is faster than tethering of floaters, as expected from the high linker density of the receptors. This linear relationship allowed accurate control of NP density on lipid bilayers. We also observed that the NPs loaded in the linear range were in better quality; floater particles were more mobile, and less aggregation of NPs was observed. We speculate that NPs could non-specifically bind to a lipid bilayer when incubation time is too long (beyond the linear range). (**B**) The number of tethered NPs in three replicate flow chambers (i.e. tablets). Tethering of G-NRs and B-NRs (left), and B-NRs and G-NFs (right). For each tablet, the number of NPs was counted in an area of 90 × 90 μm^2 at four different positions after the tethering. Error bars indicate standard deviations calculated based on the particle

numbers obtained from the four different positions. The tablet-to-tablet variability in particle numbers was negligible. (**C**) The number of three different NPs (B-NRs, G-NRs, and G-NFs) measured at four different positions in a flow chamber. Error bars indicate standard deviation calculated based on the number of NPs obtained from the four different positions. These results demonstrate that the tethering of NPs on a lipid nanotablet is controllable and robust across the large area of lipid bilayers, regardless of nanoparticle types and mobility. The typical population density used in this study was approximately 3,700 receptors and 300 floaters per 180 × 180 μm^2. This optimum density was chosen because (*i*) it was desirable to observe at least 300 binding or unbinding events within 30 min and (*ii*) at a higher density signal overlaps compromised the accuracy of the image analysis. (**D**) Degree of multimer-forming reactions estimated by MATLAB-based simulation. Assembly reactions of SLB-tethered NPs were modeled and simulated using MATLAB. This computational approach was developed to estimate how a receptor/floater ratio affects the degree of multimer formation. In the model, a given number of receptors and floaters were randomly dispersed in an area of 128 × 128 μm^2 with the periodic boundary conditions. The total number of NPs in the area was set to be 1,800. Diffusion constants of floaters were assigned to have a normal distribution with mean 0.9 $\mu m^2/s$ and standard deviation of 0.3 $\mu m^2/s$. This approximation is based on the experimental data on diffusion profiles of floaters shown in fig. S3. We assumed that the diffusion of floaters is governed by a two-dimensional random walk, where the step size for each floater is $\sqrt{4Dt}$ with t = 5 ms. Positions of receptors were fixed. To run the simulation efficiently, floaters were set to diffuse on two-dimensional square lattice with cell edge that was equal to the diameter of particle cross section. The binding events between a receptor and a floater occur with the probability of 0.3 for each collision. In the simulation, “collision” is defined as an event that occurs when a coordinate of a floater overlaps with that of a receptor. For multimer formation processes, lower binding probabilities (0.18 for trimer formation and 0.09 for tetramer formation) were used because the addition of another floater to a receptor–floater dimer and a trimer is sterically less favored than the addition of a floater to a receptor (*47*). The scaling factor was introduced based on the geometrical constraints. The fraction of floaters that formed multimers (trimers or tetramers) in simulated assembly reactions for a given receptor/floater ratio was estimated using MATLAB-based simulation. Under 10:1, 8:1, 5:1, and 2:1 receptor/floater ratios, 6%, 15%, 15%, and 34% of floaters ended up forming multimers, respectively.

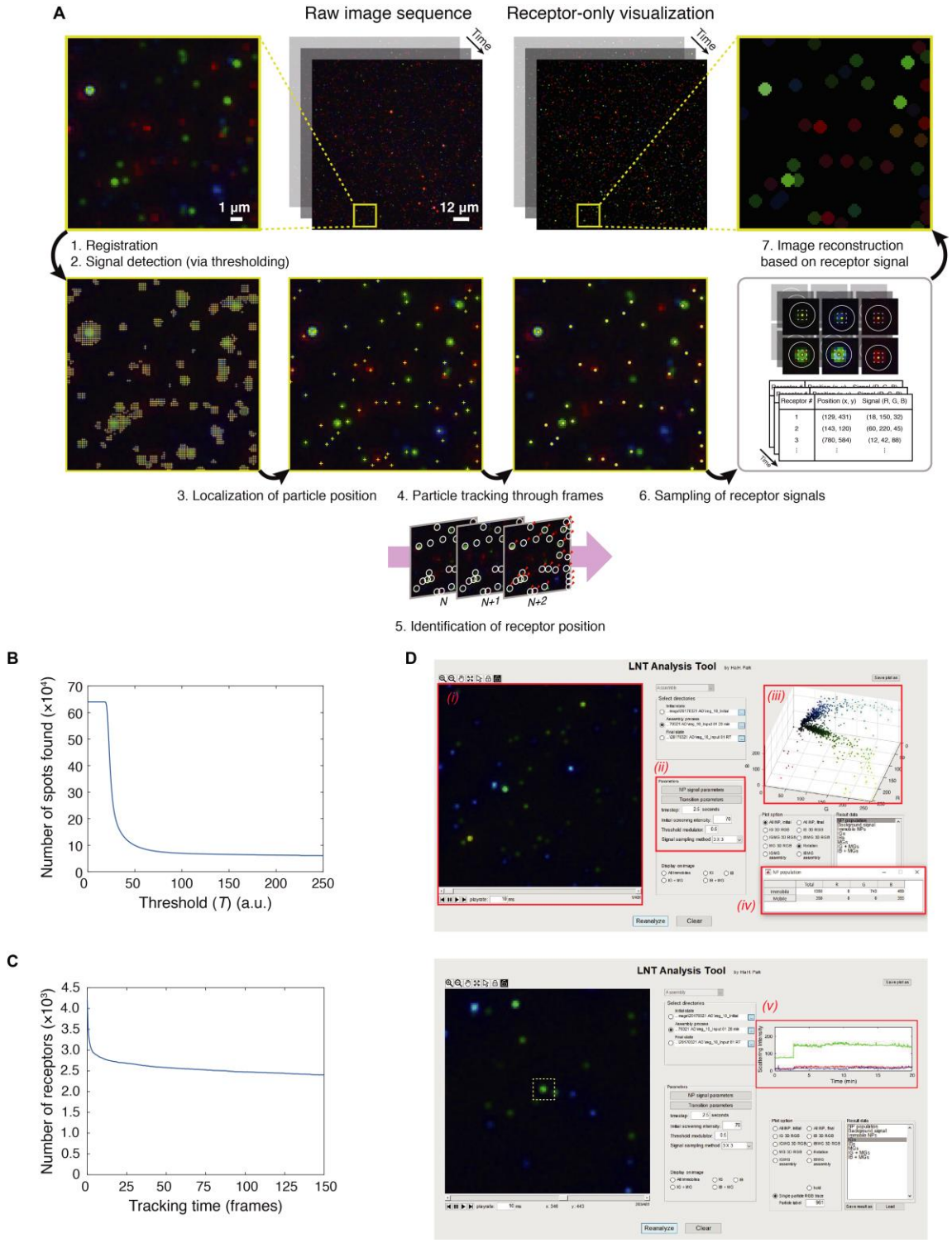

Fig. S6. Image analysis pipeline. (**A**) Single-particle tracking algorithm for the analysis of time-lapse DFM images. After image registration (step 1), pixels with signal intensities higher than a detection parameter are detected and marked with yellow crosses (step 2). The detection parameter (d) is specific to each dark-field movie because types and populations of nanoparticles on each tablet affect the background signal of the movie. In our analysis, d is defined as: $d = m_{background} + 0.5 \times \sigma_{background}$, where $m_{background}$ and $\sigma_{background}$ are average and standard deviation of the pixels whose gray scale intensities are below a chosen threshold T. The boundaries of the detected signals (pixels) are readily distinguishable. It was assumed that the segmented signals are from nanoparticles. Centers of the segmented signals are localized to provide the positions of the nanoparticles (step

3). The localized particles are marked with yellow crosses. Receptors are identified by comparing the localized positions through frames (step 4). Particles whose positions remained unchanged for entire imaging duration are identified as receptors and marked with yellow dots (step 5). For each receptor, a signal intensity is sampled and averaged from a 3 × 3 pixel window that is marked with a white dotted box. Visualizing only receptor signals in the dark background yields a "receptor-only" dark-field image sequence. (**B**) The number of detected signals plotted as a function of the threshold *T*. The presence of a plateau suggests that there is a condition over which the number of identified signals is insensitive to the threshold value *T* chosen for the analysis. (**C**) The number of receptors plotted as a function of the tracking frame. The presence of a plateau indicates that the number of identified receptors is insensitive to the particular tracking length chosen for the analysis. We chose 70 (a.u.) as a threshold *T* and 31 (frames) as a tracking length. Positions and signals of receptors in the raw dark-field image sequence movie correspond very well with those identified by the algorithm (movie S3). The comparison also shows that the algorithms reliably differentiate receptors from floaters in the high-density setting. (**D**) MATLAB-based graphical user interface for analyzing nanoparticle logic gates on LNTs. This program has the following features: (*i*) a raw dark-field image sequence uploaded for the analysis, (*ii*) a control panel for analysis parameters (e.g., threshold, signal sampling method, and transition parameter), (*iii*) a visualization of detected receptor signals in three-dimensional (3D) space of a red-green-blue (RGB) intensity scatter plot (i.e. 3D signal profile), (*iv*) the number of receptors (R-NR, G-NR, and B-NR) and floaters (R-NF, G-NF, and B-NF) detected from the input image sequence, and (*v*) a time trace of a selected receptor signal (marked with a yellow dotted box).

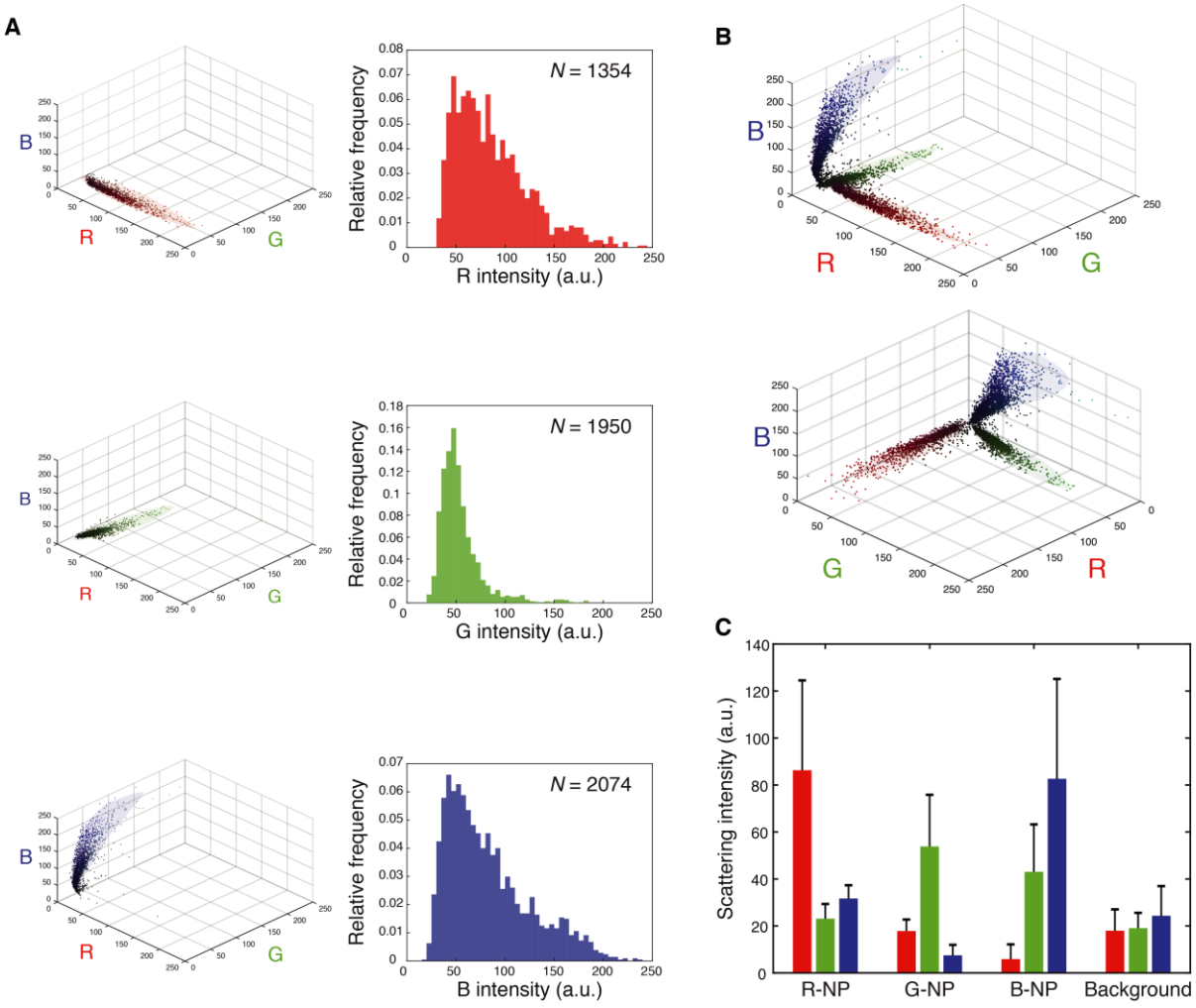

Fig. S7. Scattering signal profiles of red, green, and blue nanoparticles. (**A**) RGB intensity scatter plot of red nanoparticles (R-NPs, upper), green nanoparticles (G-NPs, middle), and blue nanoparticles (B-NPs, lower) in RGB signal space. The background of each cluster is marked with its corresponding color to allow the clusters to be easily distinguishable from each other. (**B**) RGB scattering signals from R-NPs, G-NPs, and B-NPs are visualized together in the RGB signal space. The visualization shows three signal clusters with minimal overlap. The scattering signals from the red, green, and blue nanoparticles are readily distinguishable from each other. **(C**) Average red, green, and blue scattering intensities of the nanoparticles and background signals are represented with red, green, and blue bars. Error bars indicate standard deviations. The signal profiles of the three core nanoparticles were obtained by the image analysis algorithm (described in fig. S6) and used in identifying and classifying logic-gated nanoparticle reactions.

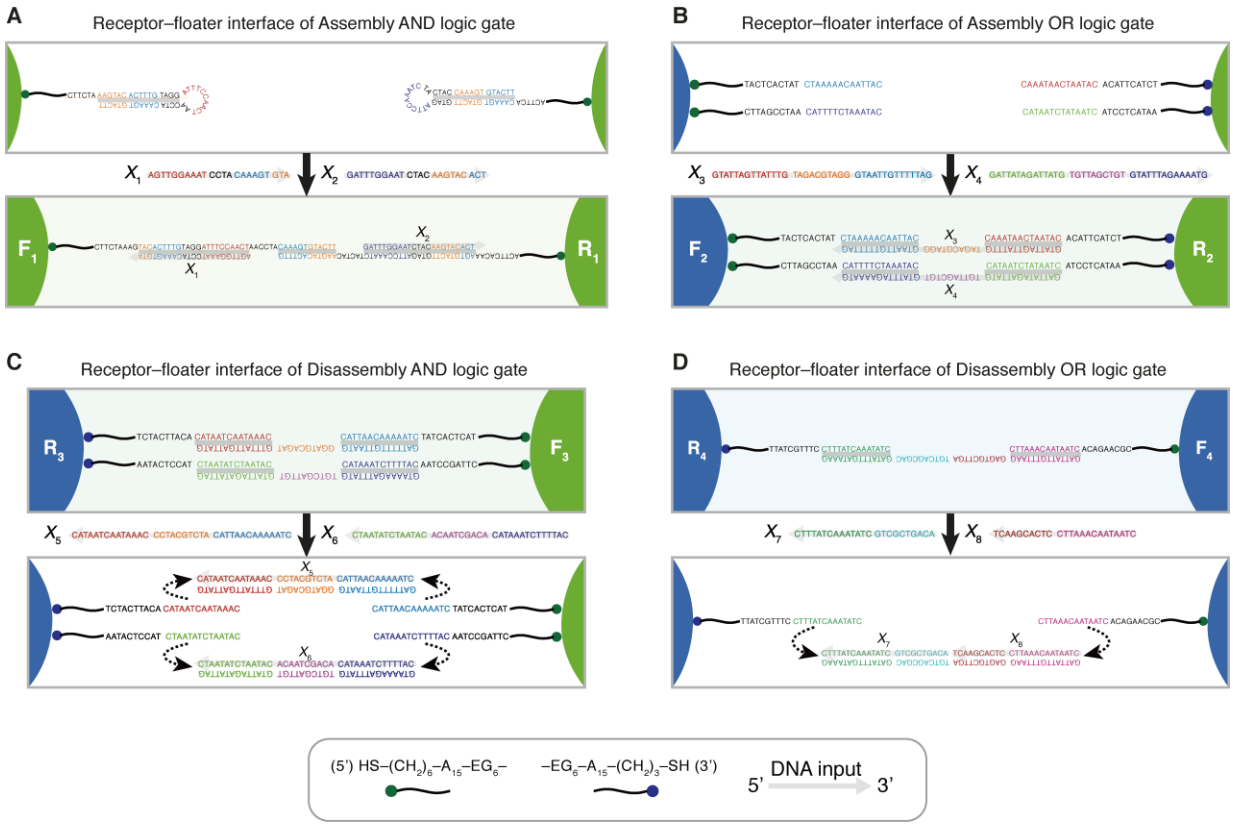

Fig. S8. Nucleotide-level schematics of two-input logic gates. (**A**) Two-input Assembly AND gate. (**B**) Two-input Assembly OR gate. (**C**) Two-input Disassembly AND gate. (**D**) Two-input Disassembly OR gate. The sequence-level illustrations show how the gates respond to molecular inputs. EG denotes an ethylene glycol unit.

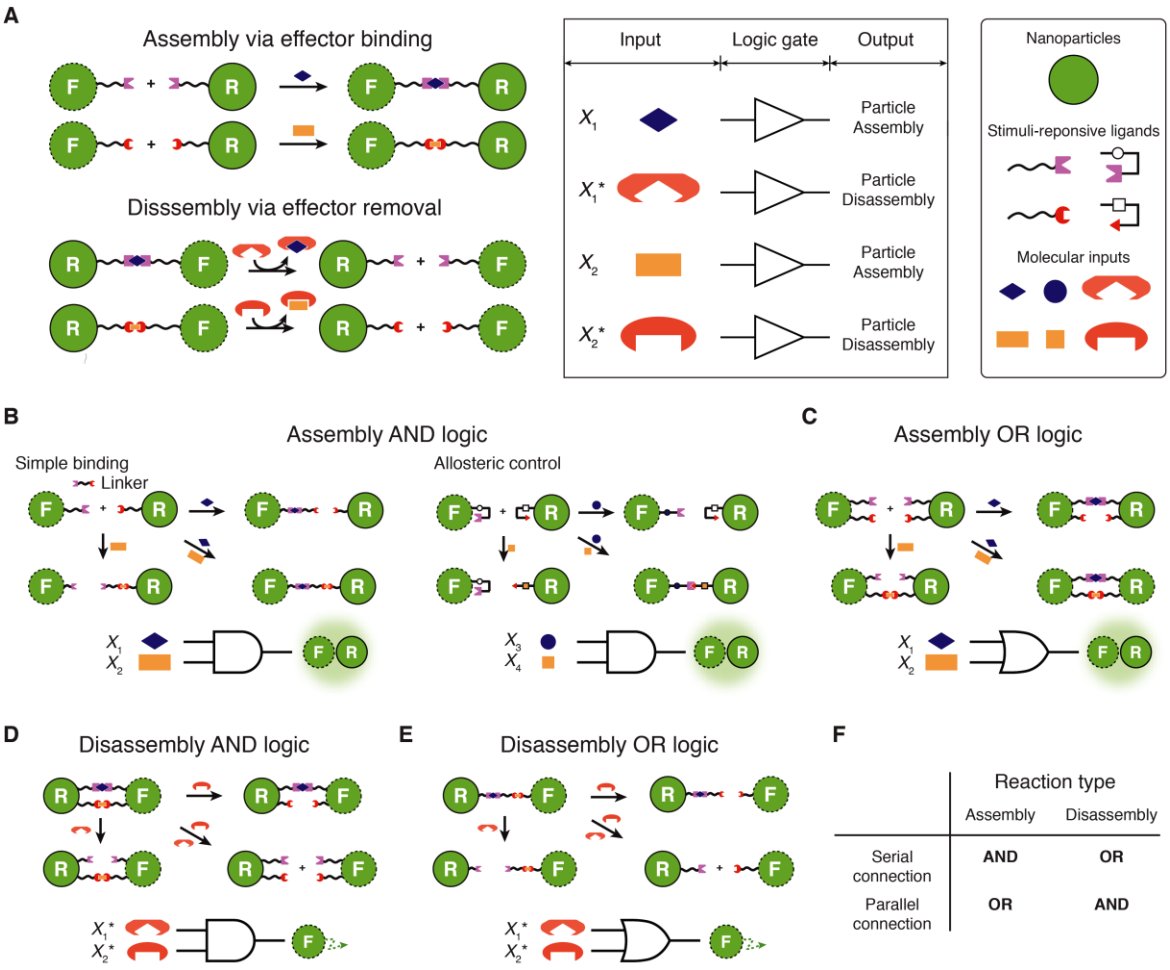

Fig. S9. Design principles for nanoparticle logic gates. (**A**) Graphical summary of the generalizable concept. Illustration of effector-mediated nanoparticle Assembly/Disassembly YES gates (left) and truth table for the concept (right) are provided. Selective effector-ligand pair and effector-chelator pair are required for construction of Assembly/Disassembly logic gates. To build a logic gate using two nanoparticles, "bonding" interactions in the receptor–floater interface need to be programmed in such a way that the bonds are formed (via assembly) or cleaved (via disassembly) only if two molecular inputs satisfy AND or OR logic. (**B**) Two-input Assembly AND gate. (**C**) Two-input Assembly OR gate. Assembly reactions are controlled by AND logic when the bond-forming interaction require the *serial* activation by the two inputs and by OR logic when the bond-forming interaction is controlled in *parallel*. (**D**) Two-input Disassembly AND gate. (**E**) Two-input Disassembly OR gate. Similarly, Disassembly reactions are modulated by AND logic via parallel disconnection and by OR logic via serial disconnection. (**F**) Table summary. These illustrations describe the generalized concept of the interface programming. In this study, we used sequence recognition and strand displacement of DNA as the mechanisms to implement the logic. Specifically, we used single-stranded DNA molecules as effectors, thiolated oligonucleotides as ligands, and a strand displacement as chelation mechanism. We foresee that this design rules can be potentially applied to other ligand systems and core nanostructures.

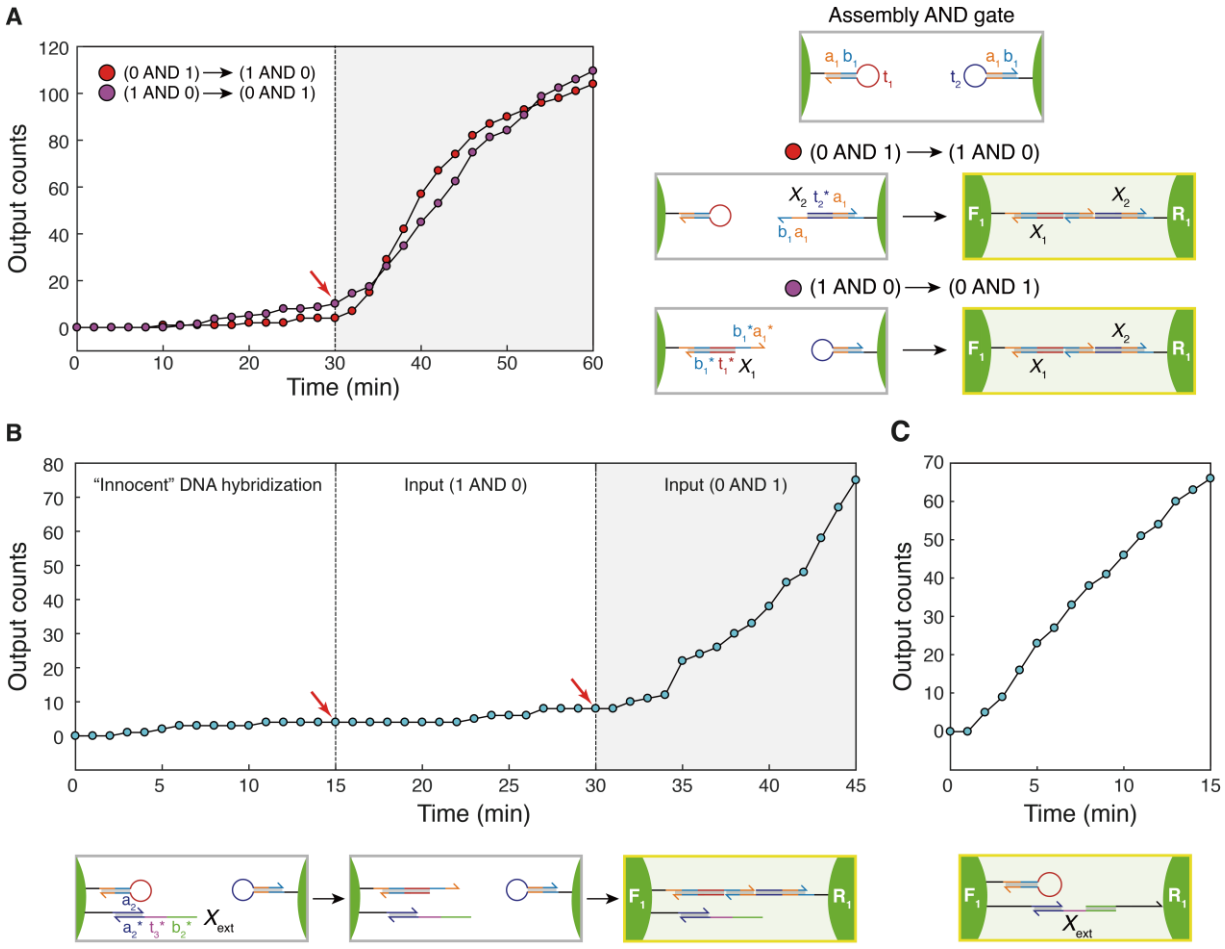

Fig. S10. Modularity of a hairpin-based two-input Assembly AND gate. (**A**) Sequential activation of the two-input Assembly AND gate (described in Fig. 2A and fig. S8A). The responses of the Assembly AND gate to sequentially introduced inputs (Red: X_2 addition followed by X_1 addition. Magenta: X_1 addition followed by X_2 addition). Two hybridization events are all required to induce assembly reactions between R_1 and F_1. (**B**) Operation of the Assembly AND gate after hybridization by an "innocent" DNA input X_{ext} that interacts with a non-hairpin ligand on F_1. The hairpin-based assembly is insensitive to other hybridization events on the same particle. (**C**) Assembly by the DNA input X_{ext}. The assembly by the simple hybridization (as in Assembly YES gate) is insensitive to the presence of hairpin ligands on the same particle. In addition to the time-versus-output plots, domain-level illustrations are provided. DNA sequences and experimental conditions are listed in tables S2 and S3.

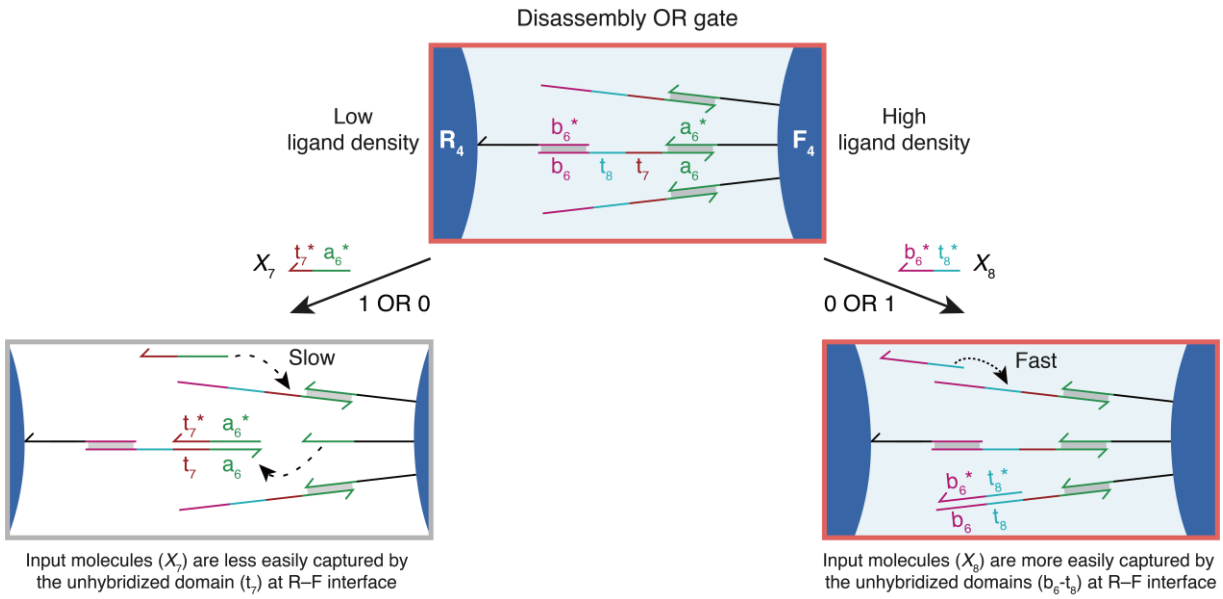

Fig. S11. Uneven responses of a two-input Disassembly OR gate. We speculate that the higher response rate under 1 OR 0 condition than the response rate under 0 OR 1 condition is attributed to the higher density of surface ligands in F_4 than in R_4. Due to its higher ligand density, F_4 exposes more single-stranded domains (b_6-t_8-t_7) than R_4 after pre-dimerization. The exposed strands can interact with incoming input strands. In 0 OR 1 condition, interactions between the input X_8 (b_6*-t_8*) and the exposed bonds are more effective compared with those between the input X_7 (a_6*-t_7*) and the bonds in 1 OR 0 condition, mainly because the recognizable sequence is longer and more accessible for the former interaction. As a result, the input X_8 is more easily trapped by the exposed strands without leading to effective strand displacements that induce particle disassembly. This interaction is an example of undesirable interactions that occur at particle–particle interfaces. R_4, F_4, X_7, and X_8 are from Fig. 3D.

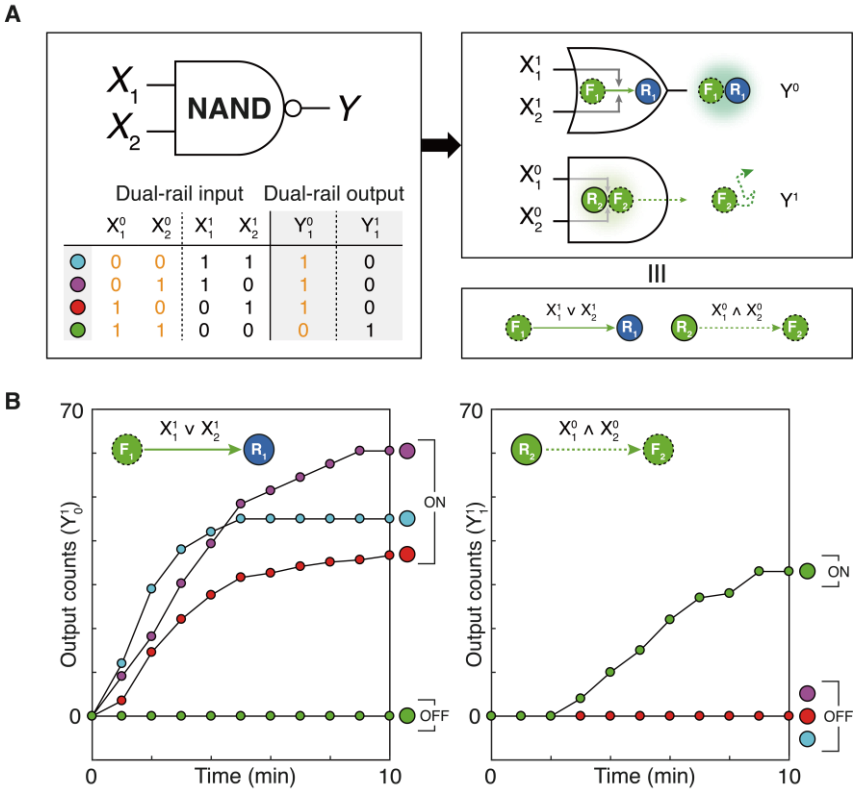

Fig. S12. A dual-rail NAND gate. (**A**) A two-input dual-rail NAND gate. Dual-rail inputs of X_i are represented as X_i^0 and X_i^1 (which denote logic FALSE and TRUE, respectively). Outputs were denoted by the same rule. A two-input Assembly OR gate (X_1^1 OR X_2^1) and a two-input Disassembly AND gate (X_1^0 AND X_2^0) are implemented in parallel to process dual-rail NAND logic. (**B**) Kinetics analysis. The two gates generate correct logic outputs without interfering with each other, providing ON/OFF levels over 37-fold (Y^0, two-input Assembly OR) and 33-fold (Y^1, two-input Disassembly AND). This result demonstrates the modularity of nanoparticle logic gates. DNA sequences and experimental conditions are listed in tables S2 and S3.

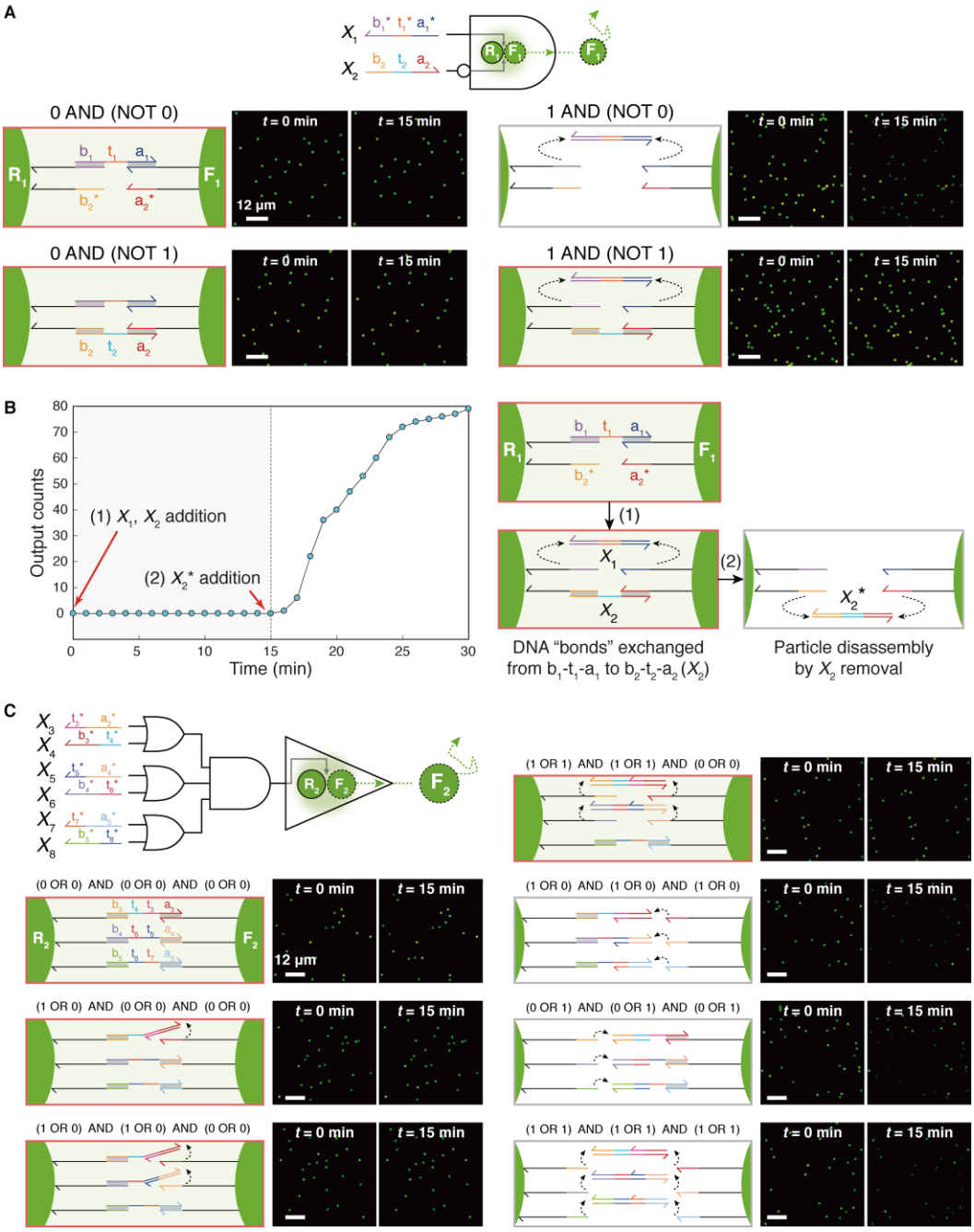

Fig. S13. Disassembly INHIBIT and six-input Disassembly gates. (**A**) Domain-level illustration (left) and reconstructed dark-field images (right) of a two-input Disassembly INHIBIT gate that evaluates X_1 AND (NOT X_2) logic. The reconstructed images provide only receptor signals. The disassembly reactions were observed only in the logical 1 AND (NOT 0) condition. (**B**) Characterization of strand displacement reactions in the Disassembly INHIBIT gate. According to the design, the DNA bond at an R_1–F_1 interface should change from b_1-t_1-a_1 to b_2-t_2-a_2 (X_2) upon the addition of the two inputs X_1 and X_2. If the bond exchange is effective at the receptor–floater interface, the disassembly reactions should occur upon the subsequent addition of X_2*. The time-versus-output plot shows that the INHIBIT gate operates as designed. DNA sequences and experimental conditions are listed in tables S2 and S3. See also movie S8. (**C**) Domain-level illustrations (left) and reconstructed dark-field images of the six-input Disassembly gate that processes (X_3 OR X_4) AND (X_5 OR X_6) AND (X_7 OR X_8) logic. DNA sequences and experimental conditions are listed in tables S2 and S3. See also movie S9.

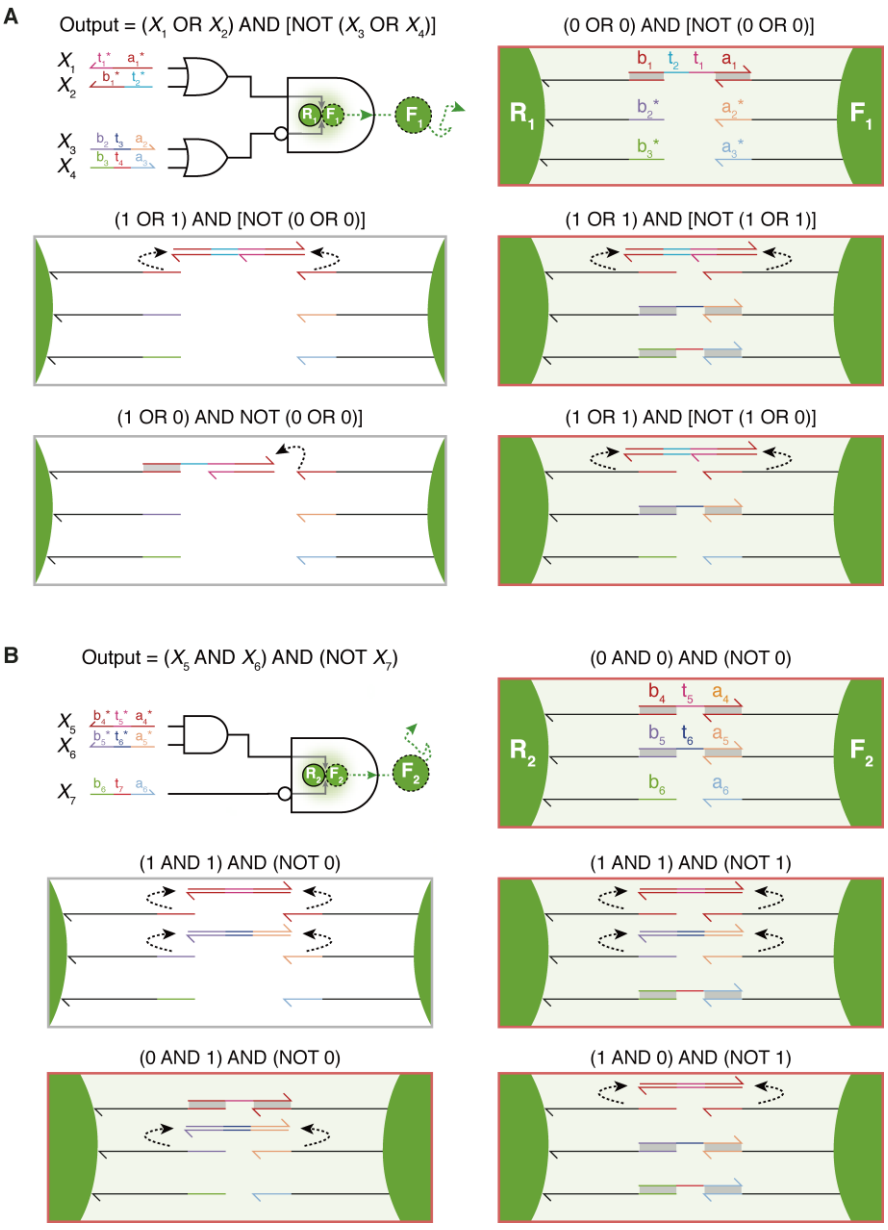

Fig. S14. Complex multi-input Disassembly gates. The approaches used to realize the INHIBIT logic and fan-in were combined to design Disassembly gates with more complex logic expressions. (**A**) A four-input Disassembly gate that processes (X_1 OR X_2) AND [NOT (X_3 OR X_4)] logic expression. In this design, either X_1 or X_2 can cleave a DNA bond (in a pre-formed R_1–F_1 dimer) and either X_3 or X_4 can form a bond within the dimer. For disassembly of the dimer, bond cleavage reactions should proceed in the absence of X_3 and X_4. (**B**) A three-input Disassembly gate that processes (X_5 AND X_6) AND (NOT X_7) logic. For disassembly of the dimer, X_5 and X_6 are required to remove the two different DNA bonds without additional bond formations by X_7.

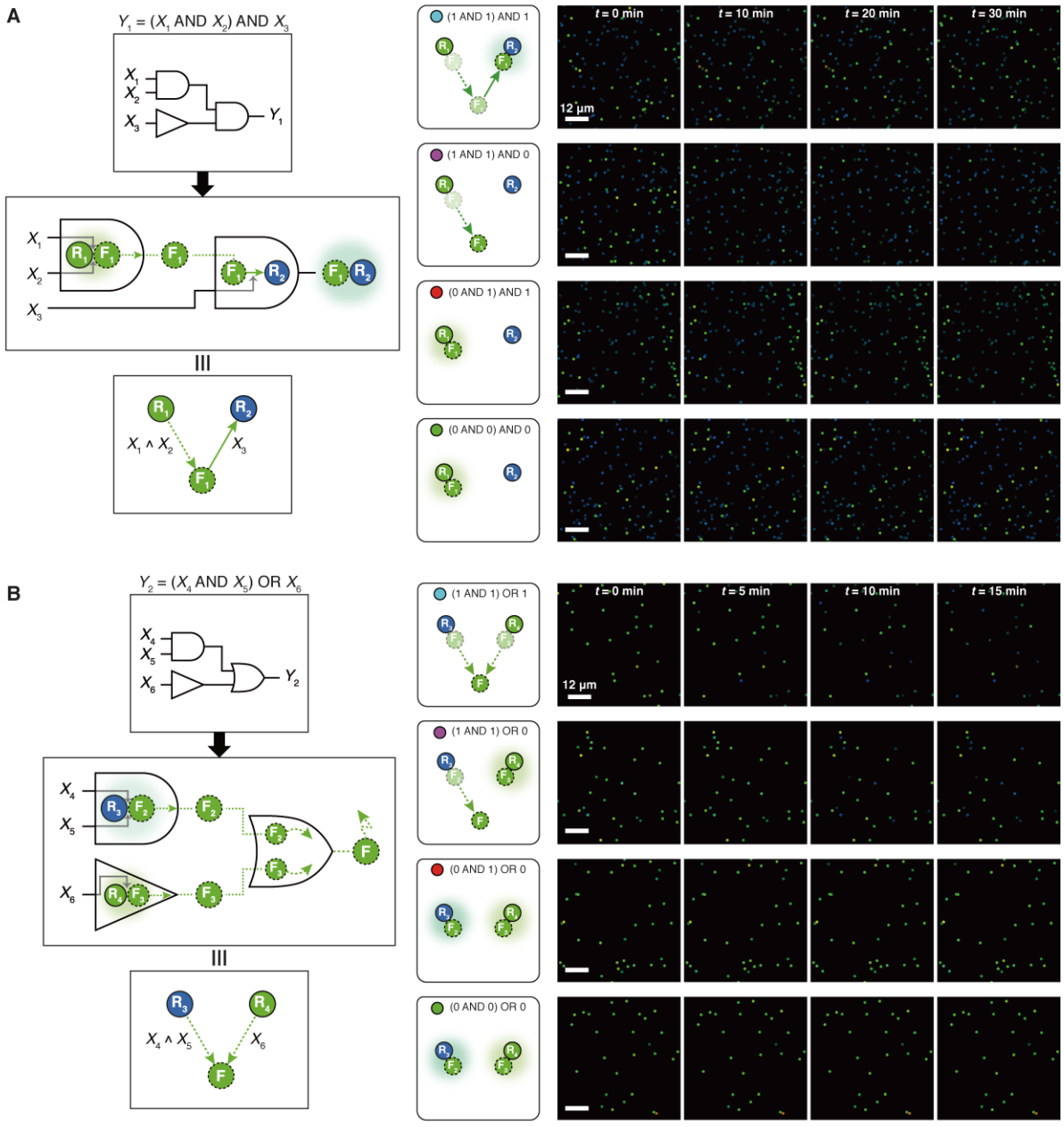

Fig. S15. Dark-field snapshots of two-layer AND-AND and AND-OR cascade circuits. (**A**) Two-layer AND-AND cascade circuit. The release of G-NFs (F_1) from G-NRs (R_1) is controlled by AND logic (X_1 AND X_2). The released F_1 can bind to R_2 only when the assembly input X_3 is present. The final circuit output is controlled by the three-input logic expression (X_1 AND X_2) AND X_3. In the first condition (1 AND 1) AND 1, the green intensity decreases in R_1 and increases in R_2, showing the successful cascading by the G-NFs (F_1). In the second condition (1 AND 1) AND 0, only the decrease in green intensity is observed. The lack of signal increase indicates that the released floaters (F_1) do not bind to other receptors. The bottom two conditions show no visible responses. See also movie S11. (**B**) Two-layer AND-OR cascade circuit. The release of G-NFs (F_2) from B-NRs (R_3) is controlled by AND logic (X_4 AND X_5), and the release of different G-NFs (F_3) from G-NRs (R_4) is controlled by YES logic (X_6). The final circuit output is controlled by the three-input logic expression (X_4 AND X_5) OR X_6. In the first condition (1 AND 1) OR 1, the green intensity decrease from both R_3 and R_4, showing the successful release of the G-NFs from each receptor. In the second condition (1 AND 1) OR 0, the decrease in green intensity is only observed in B-NRs. This result indicates the dissociation of R_3–F_2 pairs are controlled by the AND logic operation. The bottom two conditions show no visible responses. See also movie S12.

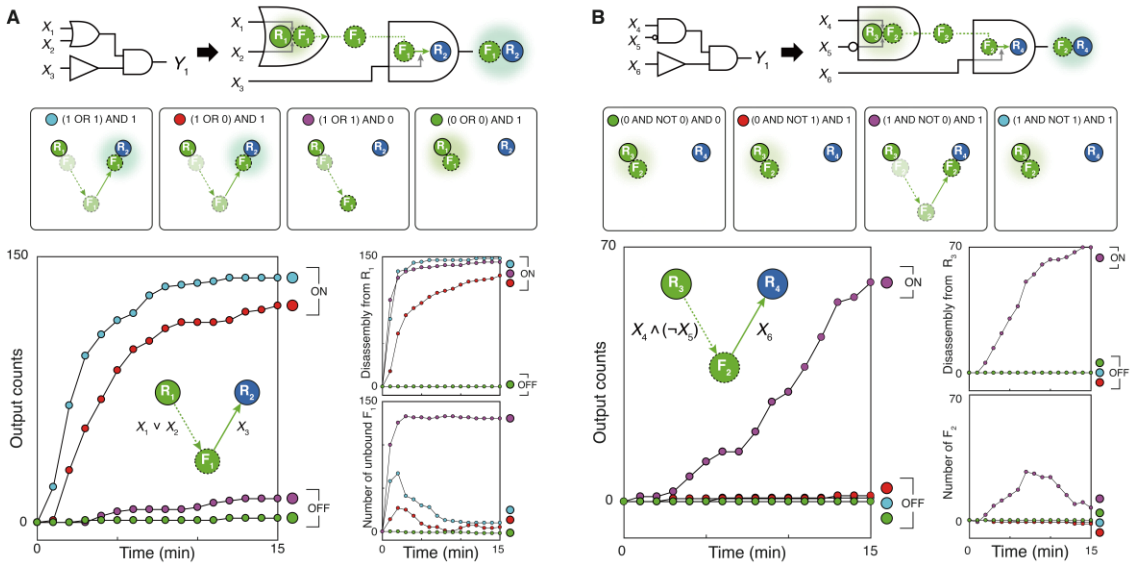

Fig. S16. Two-layer OR-AND and INHIBIT-AND cascade circuits. (**A**) Two-layer OR-AND cascade circuit. The network-level AND wiring scheme is applied to construct a nanoparticle circuit that performs (X_1 OR X_2) AND X_3 logic operations. The circuit generates correct outputs that correspond to its logic, providing an ON/OFF level over 11-fold. The upstream Disassembly gate exhibited an ON/OFF level over 128-fold. As in the AND-AND cascade circuit shown in Fig. 4B, the population dynamics of G-NFs (F_1) was estimated in the circuit. The analysis showed that the G-NFs released from G-NRs (R_1) are bound to B-NRs (R_2) only when the input X_3 required for the assembly reaction is present. (**B**) Two-layer INHIBIT-AND cascade circuit. Disassembly reactions between G-NRs (R_3) and G-NFs (F_2) are controlled by (X_4 AND NOT X_5) logic, and the subsequent assembly reactions of F_2 with B-NRs (R_4) are mediated by input X_6. Generation of F_2-R_4 dimers is thus controlled by (X_4 AND NOT X_5) AND X_6 logic expression. The circuit carried out logic operations as designed, resulting in an ON/OFF level over 37-fold. The upstream INHIBIT gate provided an ON/OFF level over 70-fold. These results indicate that the released F_2 are bound to B-NRs only in the presence of input X_6. DNA sequences and experimental conditions are listed in tables S2 and S3.

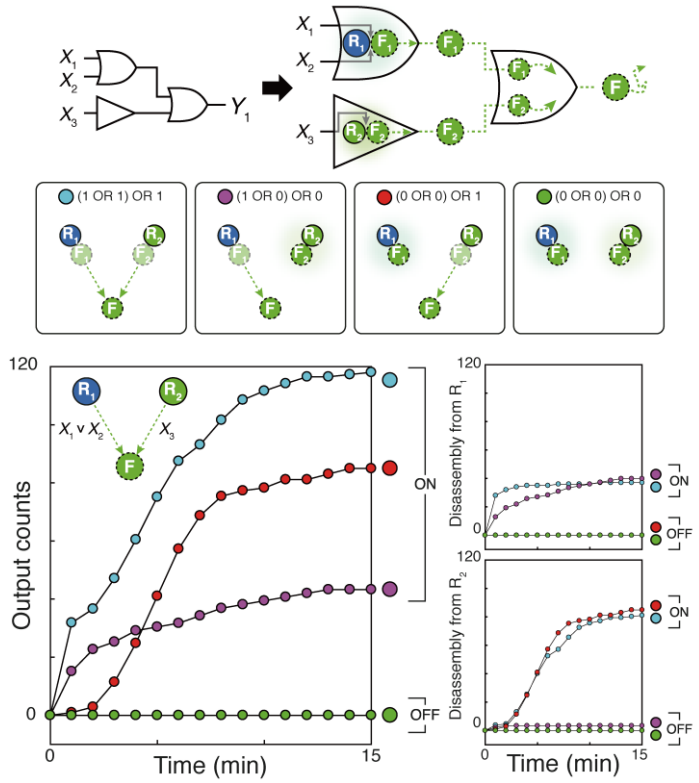

Fig. S17. A two-layer OR-OR cascade circuit. The network-level OR wiring scheme is applied to construct a nanoparticle circuit that performs (X_1 OR X_2) OR X_3 logic operations. The circuit performs the computation as designed, resulting in an ON/OFF level over 43-fold. The upstream Disassembly OR gate and YES gate provided ON/OFF levels over 37-fold and 24-fold, respectively. DNA sequences and experimental conditions are listed in tables S2 and S3.

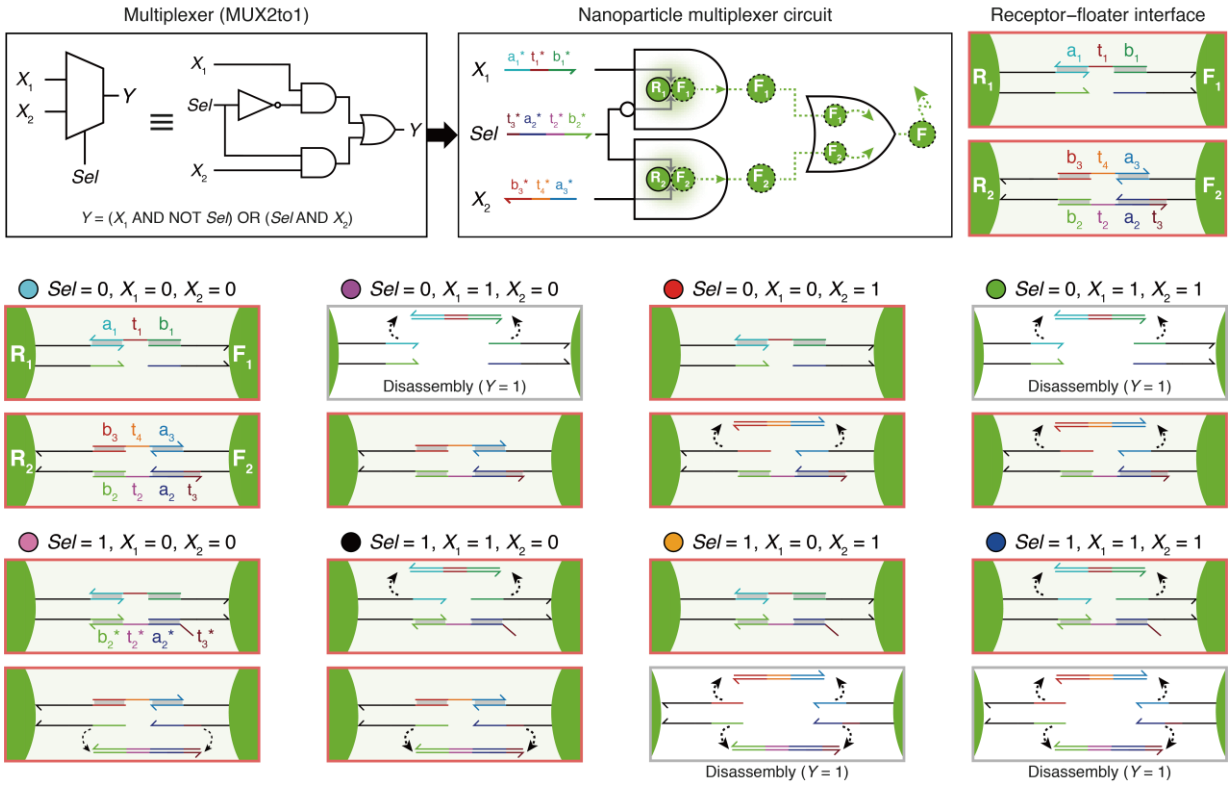

Fig. S18. A nanoparticle multiplexer circuit. A multiplexer circuit was constructed by wiring a two-input Disassembly INHIBIT gate (R_1–F_1) and a two-input Disassembly AND gate (R_2–F_2) with OR logic. The circuit takes three inputs X_1, *Sel*, and X_2 and releases G-NFs as outputs. The nanoparticle surface ligands were designed in a way that two different receptor–floater pairs could simultaneously process the Selector (*Sel*) strands. In this design, spontaneous interactions between R_1 and R_2, as well as those between F_1 and F_2 could occur. However, these undesirable interactions were prevented by loading the nanoparticle circuit components in a specific order and by introducing the protection strand a_2. Domain-level illustration of the circuit operations is provided. DNA sequences and experimental conditions are listed in tables S2 and S3. See also movie S13.

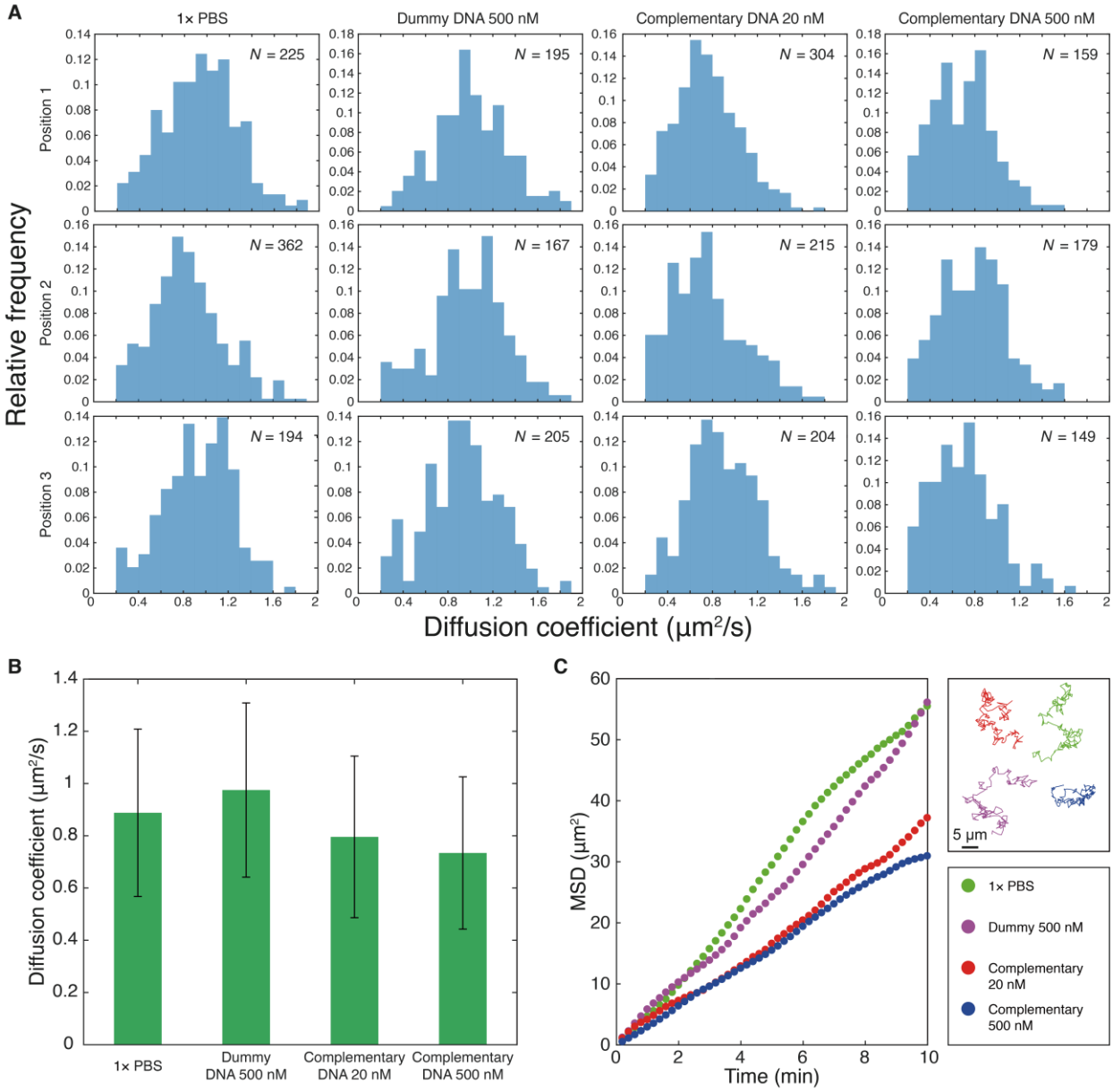

Fig. S19. Effect of DNA concentration on floater diffusion. Diffusions of G-NFs were analyzed in various contexts, such as in 1× PBS buffer, with a high concentration (500 nM) of "dummy" DNA, with a low concentration (20 nM) of complementary DNA inputs, and with a high concentration (500 nM) of complementary DNA inputs. There was no complementarity between the surface ligands of the G-NFs and the dummy DNA (5'- GTTTAAGATTTATG GTTAAGCGTA GATTAAGTATTAAG -3'). The G-NFs used in the Assembly YES gate were used for analysis. In each solution, the diffusions of the floater were analyzed in three different positions. (**A**) Histograms of diffusion coefficients of the G-NFs under each condition. (**B**) Diffusion coefficient of the G-NFs. Error bars indicate standard deviation of the diffusion coefficients in each condition. (**C**) MSD versus time plots of the four representative diffusion trajectories. The analysis showed that the overall diffusive behaviors of G-NFs are robust to the chemical environments of the solution.

Table S1. Response rates of two-input logic gates.

Logic Circuit	Input condition			
	00	01	10	11
Two-input Assembly AND gate	2.80	7.78	17.74	84.31
Two-input Assembly OR gate	0.817	76.90	71.66	79.22
Two-input Disassembly AND gate	0	0.90	0	83.46
Two-input Disassembly OR gate	0	42.35	74.24	79.00

Table S2. DNA sequences of thiolated strands used for functionalizing nanoparticles. *r*: a surface density of a thiolated DNA strand. Spacer for linker and ligand with 5' thiol group: 5'- $(CH_2)_6$–A_{15}–EG_6 -3'. Spacer for linker and ligand with 3' thiol group: 5'- EG_6–A_{15}–$(CH_2)_3$ -3'.

Figure 1

Logic Circuit	NP	Ligand		Linker	
		Sequence	*r* (%)	Sequence	*r* (%)
Assembly YES gate	R (G-NR)	5'-CTATAAACTATTTC CTTTGCTATT–Spacer–SH -3'	65	5'- biotin– CTCTCTGCCTCGTTC AGACAAAACTCATCCTACT–Spacer–SH -3'	35
	F (G-NF)	5'-HS–Spacer–CGCAAAGACA CTAATAACAAATTC -3'	99.5	5'-HS–Spacer–TTACTACACTG TCACTGATCATCGCATGCTAT AC–biotin -3'	0.5
Disassembly YES gate	R (G-NR)	5'-CTATAAACTATTTC CTTTGCTATT–Spacer–SH -3'	65	5'-biotin–CTCTCTGCCTCGTT CAGACAAAACTCATCCTACT–Spacer–SH -3'	35
	F (G-NF)	5'-HS–Spacer–CGCAAAGACA CTAATAACAAATTC -3'	99.5	5'-HS–Spacer–TTACTACACT GTCACTGATCATCGCATGCTA TAC–biotin -3'	0.5

Figure 2

Logic Circuit	NP	Ligand		Linker	
		Sequence	*r* (%)	Sequence	*r* (%)
Two-input Assembly AND gate	R_1 (G-NR)	5'-HS–Spacer–ACTTCACAA AGTGTACTTGTAGATTC CAAATCTACTACAAGTAC ACT TTG -3'	65	5'-HS–Spacer–TTACTACACT GTCACTGATCATCGCATGCT ATAC–biotin -3'	35
	F_1 (G-NF)	5'-HS–Spacer–CTTCTAAAG TACACTTTGTAGGATTTC CAACTAACCTACAAAGT GTA CTT -3'	65	5'-HS–Spacer–TTACTACACT GTCACTGATCATCGCATGCT ATAC–biotin -3'	0.5
		5'-HS–Spacer–TTACTACA CTGTCACTGATCATCGCAT GCTATAC -3'	34.5		
Two-input Assembly OR gate	R_2 (G-NR)	5'-CAAATAACTAATAC ACATTCATCT–Spacer–SH -3'	32.5	5'-biotin–CTCTCTGCCTCGTT CAGACAAAACTCATCCTACT –Spacer–SH -3'	35
		5'-CATAATCTATAATC ATCCTCATAA–Spacer–SH -3'	32.5		
	F_2 (B-NF)	5'-HS–Spacer–TACTCACTAT CTAAAAACAATTAC -3'	49.75	5'-HS–Spacer–TTACTACACT GTCACTGATCATCGCATGCT ATAC–biotin -3'	0.5
		5'-HS–Spacer–CTTAGCCTAA CATTTTCTAAATAC -3'	49.75		
Two-input Disassembly AND gate	R_3 (B-NR)	5'-CAAATAACTAATAC ACATTCATCT–Spacer–SH -3'	25	5'-biotin–CTCTCTGCCTCGTT CAGACAAAACTCATCCTACT –Spacer–SH -3'	50
		5'-CATAATCTATAATC ATCCTCATAA–Spacer–SH -3'	25		
	F_3 (G-NF)	5'-HS–Spacer–TACTCACTAT CTAAAAACAATTAC -3'	49.75	5'-HS–Spacer–TTACTACACT GTCACTGATCATCGCATGCT ATAC–biotin -3'	0.5
		5'-HS–Spacer–CTTAGCCTAA CATTTTCTAAATAC -3'	49.75		

Two-input Disassembly OR gate	R_4 (B-NR)	5’-CTATAAACTATTTC CTTTGCTATT–Spacer–SH -3’	50	5’-biotin–CTCTCTGCCTCGTT CAGACAAAACTCATCCTACT –Spacer–SH -3’	50
	F_4 (B-NF)	5’-HS–Spacer–CGCAAAGA CA CTAATAACAAATTC -3’	99.5	5’-HS–Spacer–TTACTACA CTGTCACTGATCATCGCATG CTATAC–biotin -3’	0.5

Figure 3

Logic Circuit	NP	Ligand		Linker	
		Sequence	*r* (%)	Sequence	*r* (%)
Two-input Disassembly INHIBIT gate	R_1 (G-NR)	5’-CAAATAACTAATAC ACATTCATCT–Spacer–SH -3’	32.5	5’-biotin–CTCTCTGCCTCGTT CAGACAAAACTCATCCTACT –Spacer–SH -3’	35
		5’-CATAATCTATAATC ATCCTCATAA–Spacer–SH -3’	32.5		
	F_1 (G-NF)	5’-HS–Spacer–TACTCACTAT CTAAAAACAATTAC -3’	49.75	5’-HS–Spacer–TTACTACACTG TCACTGATCATCGCATGCTA TAC–biotin -3’	0.5
		5’-HS–Spacer–CTTAGCC TAA CATTTTCTAAATAC -3’	49.75		
Six-input Disassembly gate (fan-in)	R_2 (G-NR)	5’-CTATAAACTATTTC CTTTGCTATT–Spacer–SH -3’	22	5’-biotin–CTCTCTGCCTCGTT CAGACAAAACTCATCCTACT –Spacer–SH -3’	34
		5’-CAAATAACTAATAC ACATTCATCT–Spacer–SH -3’	22		
		5’-CATAATCTATAATC ATCCTCATAA–Spacer–SH -3’	22		
	F_2 (G-NF)	5’-HS–Spacer–CGCAAAGA CA CTAATAACAAATTC -3’	33.2	5’-biotin–CTCTCTGCCTCGTT CAGACAAAACTCATCCTACT –Spacer–SH -3’	0.4
		5’-HS–Spacer–TACTCACTAT CTAAAAACAATTAC -3’	33.2		
		5’-HS–Spacer–CTTAGCCTAA CATTTTCTAAATAC -3’	33.2		
Two-input Disassembly Gate with three outputs (fan-out)	R_3 (G-NR)	5’-CAAATAACTAATAC ACATTCATCT–Spacer–SH -3’	32.5	5’-biotin–CTCTCTGCCTCGTT CAGACAAAACTCATCCTACT –Spacer–SH -3’	35
		5’-CATAATCTATAATC ATCCTCATAA–Spacer–SH -3’	32.5		
	F_3 (R-NF)	5’-HS–Spacer–TACTCACTAT CTAAAAACAATTAC -3’	49.75	5’-HS–Spacer–TTACTACACTG TCACTGATCATCGCATGCTA TAC–biotin -3’	0.5
		5’-HS–Spacer–CTTAGCCTAA CATTTTCTAAATAC -3’	49.75		
	F_4 (G-NF)	5’-HS–Spacer–TACTCACTAT CTAAAAACAATTAC -3’	49.75	5’-HS–Spacer–TTACTACACTG TCACTGATCATCGCATGCTA TAC–biotin -3’	0.5
		5’-HS–Spacer–CTTAGCCTAA CATTTTCTAAATAC -3’	49.75		
	F_5 (B-NF)	5’-HS–Spacer–TACTCACTAT CTAAAAACAATTAC -3’	49.75	5’-HS–Spacer–TTACTACACTG TCACTGATCATCGCATGCTA TAC–biotin -3’	0.5
		5’-HS–Spacer–CTTAGCCTAA CATTTTCTAAATAC -3’	49.75		

Figure 4

Logic Circuit	NP	Ligand		Linker	
		Sequence	*r* (%)	Sequence	*r* (%)
AND-AND Cascade	R_1 (G-NR)	5'-CAAATAACTAATAC ACATTCATCT–Spacer–SH -3'	32.5	5'-biotin–CTCTCTGCCTCGTT CAGACAAAACTCATCCTACT –Spacer–SH -3'	35
		5'-CATAATCTATAATC ATCCTCATAA–Spacer–SH -3'	32.5		
	F_1 (G-NF)	5'-HS–Spacer–TACTCACTAT CTAAAAACAATTAC -3'	33.2	5'-HS–Spacer–TTACTACACTG TCACTGATCATCGCATGCTA TAC–biotin -3'	0.4
		5'-HS–Spacer–CTTAGCCTAA CATTTTCTAAATAC -3'	33.2		
		5'-HS–Spacer–CGCAAAGACA CTAATAACAAATTC -3'	33.2		
	R_2 (B-NR)	5'-CTATAAACTATTTC CTTTGCTATT–Spacer–SH -3'	50	5'-biotin–CTCTCTGCCTCGTT CAGACAAAACTCATCCTACT –Spacer–SH -3'	50
AND-OR Cascade	R_3 (B-NR)	5'-CATAATCTATAATC ATCCTCATAA–Spacer–SH -3'	25	5'-biotin–CTCTCTGCCTCGTT CAGACAAAACTCATCCTACT –Spacer–SH -3'	50
		5'-CATTATCATATAAC TCAACGTCAC–Spacer–SH -3'	25		
	F_2 (G-NF)	5'-HS–Spacer–CTTAGCCTAA CATTTTCTAAATAC -3'	49.75	5'-HS–Spacer–TTACTACACTG TCACTGATCATCGCATGCTA TAC–biotin -3'	0.5
		5'-HS–Spacer–AATCAGC ATCCTATTACATAATTC -3'	49.75		
	R_4 (G-NR)	5'-CTATAAACTATTTC CTTTGCTATT–Space–SH -3'	65	5'-biotin–CTCTCTGCCTCGTT CAGACAAAACTCATCCTACT –Spacer–SH -3'	35
	F_3 (G-NF)	5'-HS–Spacer–CGCAAAGACA CTAATAACAAATTC -3'	99.5	5'-HS–Spacer–TTACTACACTG TCACTGATCATCGCATGCTA TAC–biotin -3'	0.5

Figure 5

Logic Circuit	NP	Ligand		Linker	
		Sequence	*r* (%)	Sequence	*r* (%)
Multiplexer	R_1 (B-NR)	5'-HS–Spacer–CGCAAAGACA CTAATAACAAATTC -3'	32.5	5'-HS–Spacer–TTACTACACTG TCACTGATCATCGCATGCTA TAC–biotin -3'	35
		5'-HS–Spacer–CTGCACATTA GTATTAGTTATTTG	32.5		
	F_1 (G-NF)	5'-CTATAAACTATTTC CTTTGCTATT–Spacer–SH -3'	49.75	5'-biotin–CTCTCTGCCTCGTT CAGACAAAACTCATCCTACT –Spacer–SH -3'	0.5
		5'-GTAATTGTTTTTAG TATTCTTCTC–Spacer–SH -3'	49.75		
	R_2 (G-NR)	5'-CAAATAACTAATAC ACATTCATCT–Spacer–SH -3'	32.5	5'-biotin–CTCTCTGCCTCGTT CAGACAAAACTCATCCTACT –Spacer–SH -3'	35
		5'-CATAATCTATAATC ATCCTCATAA–Spacer–SH -3'	32.5		
	F_2 (G-NF)	5'-HS–Spacer–TACTCACTAT CTAAAAACAATTAC -3'	49.75	5'-HS–Spacer–TTACTACACTG TCACTGATCATCGCATGCTA TAC–biotin -3'	0.5
		5'-HS–Spacer–CTTAGCCTAA CATTTTCTAAATAC -3'	49.75		

Figure S10B

Logic Circuit	NP	Ligand		Linker	
		Sequence	*r* (%)	Sequence	*r* (%)
Two-input Assembly AND gate	R_1 (G-NR)	5'-HS–Spacer–ACTTCACAA AGTGTACTTGTAGATTC CAAATCTACTACAAGTAC ACT TTG -3'	65	5'- HS–Spacer–TTACTACACTG TCACTGATCATCGCATGCTA TAC–biotin -3'	35
	F_1 (G-NF)	5'-HS–Spacer–CTTCTAAAG TACACTTTGTAGGATTTC CAACTAACCTACAAAGT GTACTT -3'	49.75	5'- HS–Spacer–TTACTACACTG TCACTGATCATCGCATGCTA TAC–biotin -3'	0.5
		5'-HS–Spacer–CTTAGCCTAA CATTTTCTAAATAC -3'	49.75		

Figure S10C

Logic Circuit	NP	Ligand		Linker	
		Sequence	*r* (%)	Sequence	*r* (%)
Two-input Assembly AND gate	R_1 (G-NR)	5'-CATAATCTATAATC ATCCTCATAA–Spacer–SH -3'	65	5'- biotin–CTCTCTGCCTCGTT CAGACAAAACTCATCCTACT –Spacer–SH -3'	35
	F_1 (G-NF)	5'- HS–Spacer–CTTCTAAAG TACACTTTGTAGGATTTCC AACTAACCTACAAAGTGT ACTT -3'	49.75	5'- HS–Spacer–TTACTACACTG TCACTGATCATCGCATGCTA TAC–biotin -3'	0.5
		5'- HS–Spacer–CTTAGCCTAA CATTTTCTAAATAC -3'	49.75		

Figure S12. Dual-rail NAND

Dual-rail NAND	NP	Ligand		Linker	
		Sequence	*r* (%)	Sequence	*r* (%)
Two-input Assembly OR (Y^0)	R_1 (B-NR)	5'-CATAATCTATAATC ATCCTCATAA–Spacer–SH -3'	25	5'- biotin–CTCTCTGCCTCGTT CAGACAAAACTCATCCTACT –Spacer–SH -3'	50
		5'-CATTATCATATAACTCA ACGTCAC–Spacer–SH -3'	25		
	F_1 (G-NF)	5'- HS–Spacer–CTTAGCCTAA CATTTTCTAAATAC -3'	49.75	5'- HS–Spacer–TTACTACACTG TCACTGATCATCGCATGCTA TAC–biotin -3'	0.5
		5'-HS–Spacer–AATCAGCA TCCTATTACATAATTC -3'	49.75		
Two-input Disassembly OR (Y^1)	R_2 (G-NR)	5'-CTATAAACTATTTC CTTTGCTATT–Spacer–SH -3'	32.5	5'- biotin–CTCTCTGCCTCGTT CAGACAAAACTCATCCTACT –Spacer–SH -3'	35
		5'-CAAATAACTAATAC ACATTCATCT–Spacer–SH -3'	32.5		
	F_2 (G-NF)	5'- HS–Spacer–CGCAAAGAC A CTAATAACAAATTC -3'	49.75	5'- HS–Spacer–TTACTACACTG TCACTGATCATCGCATGCTA TAC–biotin -3'	0.5
		5'- HS–Spacer–TACTCACTAT CTAAAAACAATTAC -3'	49.75		

Figure S16A. OR-AND Cascade

Logic Circuit	NP	Ligand		Linker	
		Sequence	*r* (%)	Sequence	*r* (%)
OR-AND Cascade	R_1 (G-NR)	5'-CATAATCTATAATC ATCCTCATAA–Spacer–SH -3'	65	5'- biotin–CTCTCTGCCTCGTT CAGACAAAACTCATCCTACT –Spacer–SH -3'	35
	F_1 (G-NF)	5'- HS–Spacer–CTTAGCCTAA CATTTTCTAAATAC -3'	49.75	5'- HS–Spacer–TTACTACACTG TCACTGATCATCGCATGCTA TAC–biotin -3'	0.5
		5'-HS–Spacer–CGCAAAGA CA CTAATAACAAATTC -3'	49.75		
	R_2 (B-NR)	5'-CTATAAACTATTTC CTTTGCTATT–Spacer–SH -3'	50	5'- biotin–CTCTCTGCCTCGTT CAGACAAAACTCATCCTACT –Spacer–SH -3'	50

Figure S16B. INHIBIT-AND Cascade

Logic Circuit	NP	Ligand		Linker	
		Sequence	*r* (%)	Sequence	*r* (%)
INHIBIT-AND Cascade	R_3 (G-NR)	5'-CAAATAACTAATAC ACATTCATCT–Spacer–SH -3'	32.5	5'- biotin– CTCTCTGCCTCGTT CAGACAAAACTCATCCTACT –Spacer–SH -3'	35
		5'-CATAATCTATAATC ATCCTCATAA–Spacer–SH -3'	32.5		
	F_2 (G-NF)	5'-HS–Spacer–TACTCACTAT CTAAAAACAATTAC -3'	33.2	5'- HS–Spacer–TTACTACACTG TCACTGATCATCGCATGCTA TAC–biotin -3'	0.4
		5'-HS–Spacer–CTTAGCCTAA CATTTTCTAAATAC -3'	33.2		
		5'-HS–Spacer–CGCAAAGA CA CTAATAACAAATTC -3'	33.2		
	R_4 (B-NR)	5'-CTATAAACTATTTC CTTTGCTATT–Spacer–SH -3'	50	5'- biotin– CTCTCTGCCTCGTT CAGACAAAACTCATCCTACT –Spacer–SH -3'	50

Figure S17. OR-OR Cascade

Logic Circuit	NP	Ligand		Linker	
		Sequence	*r* (%)	Sequence	*r* (%)
OR-OR Cascade	R_1 (B-NR)	5'-CATAATCTATAATC ATCCTCATAA–Spacer–SH -3'	50	5'- biotin–CTCTCTGCCTCGTT CAGACAAAACTCATCCTACT –Spacer–SH -3'	50
	F_1 (G-NF)	5'-HS–Spacer–CTTAGCCTAA CATTTTCTAAATAC -3'	99.5	5'- HS–Spacer–TTACTACACTG TCACTGATCATCGCATGCTA TAC–biotin -3'	0.5
	R_2 (G-NR)	5'-CATTATCATATAAC TCA ACGTCAC–Spacer–SH -3'	65	5'- biotin–CTCTCTGCCTCGTT CAGACAAAACTCATCCTACT –Spacer–SH -3'	35
	F_2 (G-NF)	5'-HS–Spacer–AATCAGC ATC CTATTACATAATTC -3'	99.5	5'- HS–Spacer–TTACTACACTG TCACTGATCATCGCATGCTA TAC–biotin -3'	0.5

Table S3. DNA sequences and experimental conditions used in circuit operations. Sequences are written in a 5' → 3' direction.

Figure 1

Logic Circuit	Input			Pre-dimerization	
	Name	Sequence	Condition	Sequence	Condition
Assembly YES gate	X_a	GAAATAGTTTATAG CTGCGACTGT GAATTTGTTATTAG	20 nM, 15 min	N/A	
Disassembly YES gate	X_d	CTAATAACAAATTC ACAGTCGCAG CTATAAACTATTTC	500 nM, 15 min	GAAATAGTTTATAG CTGCGACTGT GAATTTGTTATTAG	10 nM, 15 min

Figure 2

Logic Circuit	Input			Pre-dimerization	
	Name	Sequence	Condition	Sequence	Condition
Two-input Assembly AND gate	X_1	AGTTGGAAAT CCTACAAAGTGTA	100 nM, 30 min	N/A	
	X_2	GATTTGGAAT CTACAAGTACACT	100 nM, 30 min		
	X_{ext} (Fig. S10)	GATTATAGATTATG TGTTAGCTGTGTA TTTAGAAAATG	10 nM		
Two-input Assembly OR gate	X_3	GTATTAGTTATTTG TAGACGTAGG GTAATTGTTTTTAG	40 nM, 20 min	N/A	
	X_4	GATTATAGATTATG TGTTAGCTGTGTA TTTAGAAAATG	40 nM, 20 min		
Two-input Disassembly AND gate	X_5	CTAAAAACAATTAC CCTACGTCTACAA ATAACTAATAC	500 nM, 15 min	GTATTAGTTATTTG TAGACGTAGGGT AATTGTTTTTAG	40 nM, 15 min
	X_6	CATTTTCTAAATAC ACAGCTAACACAT AATCTATAATC	500 nM, 15 min	GATTATAGATTATG TGTTAGCTGTGTA TTTAGAAAATG	40 nM, 15 min
Two-input Disassembly OR gate	X_7	CTAATAACAAATTC CTCACGAACT	500 nM, 15 min	GAAATAGTTTATAG CTGCGACTGTAGT TCGTGAGGAATTT GTTATTAG	10 nM, 15 min
	X_8	ACAGTCGCAG CTATAAACTATTTC	500 nM, 15 min		

Figure 3

Logic Circuit	Input			Pre-dimerization	
	Name	Sequence	Condition	Sequence	Condition
Two-input Disassembly INHIBIT gate	X_1	CTAAAAACAATTAC CCTACGTCTA CAAATAACTAATAC	200 nM, 15 min	GTATTAGTTATTTG TAGACGTAGG GTAATTGTTTTTAG	10 nM, 15 min
	X_2	GATTATAGATTATG TGTTAGCTGT GTATTTAGAAAATG	100 nM, 15 min		
Six-input Disassembly gate (fan-in)	X_3	CTAATAACAAATTC CTCACGAACT	200 nM, 15 min	GAAATAGTTTATAG CTGCGACTGT AGTTCGTGAG GAATTTGTTATTAG	20 nM, 15 min
	X_4	ACAGTCGCAG CTATAAACTATTTC	200 nM, 15 min		
	X_5	CTAAAAACAATTAC CCTACGTCTA	200 nM, 15 min	GTATTAGTTATTTG GAAGTGTATT TAGACGTAGG GTAATTGTTTTTAG	20 nM, 15 min
	X_6	AATACACTTC CAAATAACTAATAC	200 nM, 15 min		
	X_7	CATTTTCTAAATAC ACAGCTAACA	200 nM, 15 min	GATTATAGATTATG TGGGATCTGT TGTTAGCTGT GTATTTAGAAAATG	20 nM, 15 min
	X_8	ACAGATCCCA CATAATCTATAATC	200 nM, 15 min		
Two-input Disassembly Gate with three outputs (fan-out)	X_9	CTAAAAACAATTAC CCTACGTCTA CAAATAACTAATAC	500 nM, 15 min	GTATTAGTTATTTG TAGACGTAGG GTAATTGTTTTTAG	40 nM, 15 min
	X_{10}	CATTTTCTAAATAC ACAGCTAACA CATAATCTATAATC	500 nM, 15 min	GATTATAGATTATG TGTTAGCTGT GTATTTAGAAAATG	40 nM, 15 min

Figure 4

Logic Circuit	Input			Pre-dimerization	
	Name	Sequence	Condition	Sequence	Condition
AND-AND Cascade (X_1 AND X_2) AND X_3	X_1	CTAAAAACAATTAC CCTACGTCTA CAAATAACTAATAC	500 nM, 30 min	GTATTAGTTATTTG TAGACGTAGG GTAATTGTTTTTAG	40 nM, 15 min
	X_2	CATTTTCTAAATAC ACAGCTAACA CATAATCTATAATC	500 nM, 30 min	GATTATAGATTATG TGTTAGCTGT GTATTTAGAAAATG	40 nM, 15 min
	X_3	GAAATAGTTTATAG CTGCGACTGT GAATTTGTTATTAG	100 nM, 30 min	N/A	
AND-OR Cascade (X_4 AND X_5) OR X_6	X_4	CATTTTCTAAATAC ACAGCTAACA CATAATCTATAATC	500 nM, 15 min	GATTATAGATTATG TGTTAGCTGT GTATTTAGAAAATG	40 nM, 15 min
	X_5	CTATTACATAATTC TGCATTCTTC CATTATCATATAAC	500 nM, 15 min	GTTATATGATAATG GAAGAATGCA GAATTATGTAATAG	40 nM, 15 min
	X_6	CTAATAACAAATTC ACAGTCGCAG CTATAAACTATTTC	500 nM, 15 min	GAAATAGTTTATAG CTGCGACTGT GAATTTGTTATTAG	10 nM, 15 min

Figure 5

Logic Circuit	Input			Pre-dimerization	
	Name	Sequence	Condition	Sequence	Condition
Multiplexer	X_1	CTAATAACAAATTC ACAGTCGCAG CTATAAACTATTTC	200 nM, 15 min	GAAATAGTTTATAG CTGCGACTGT GAATTTGTTATTAG	10 nM, 15 min
	X_2	CATTTTCTAAATAC ACAGCTAACA CATAATCTATAATC	500 nM, 15 min	GATTATAGATTATG TGTTAGCTGT GTATTTAGAAAATG	40 nM, 15 min
	Selector	TACTCACTAT CTAAAAACAATTAC CCTACGTCTA CAAATAACTAATAC	500 nM, 15 min	GTATTAGTTATTTG TAGACGTAGG GTAATTGTTTTTAG ATAGTGAGTA (*Sel**)	40 nM, 15 min
				GTAATTGTTTTTAG (F_2 protection)	20 nM, 15 min

Figure S10

Logic Circuit	Input			Pre-dimerization	
	Name	Sequence	Condition	Sequence	Condition
Two-input Assembly AND	X_1	AGTTGGAAATCCT ACAAAGTGTA	100 nM, 15 min	N/A	
	X_2	GATTTGGAATCTAC AAGTACACT	100 nM, 15 min		
	X_3 (Simple hybridization)	GATTATAGATTATG TGTTAGCTGT GTAT TTAGAAAATG	10 nM 15 min		

Figure S12. A dual-rail NAND gate.

Dual-rail NAND	Operation (input)			Pre-dimerization	
	Name	Sequence	Condition	Sequence	Condition
Two-input Assembly OR (Y^0)	X_1^1	GATTATAGATTATG TGTTAGCTGT GTATTTAGAAAATG	50 nM, 10 min	N/A	
	X_2^1	GTTATATGATAATG GAAGAATGCA GAATTATGTAATAG	50 nM, 10 min		
Two-input Disassembly OR (Y^1)	X_1^0	CTAATAACAAATTC ACAGTCGCAG CTATAAACTATTTC	500 nM, 10 min	GAAATAGTTTATAG CTGCGACTGT GAATTTGTTATTAG	40 nM, 15 min
	X_2^0	CTAAAAACAATTAC CCTACGTCTA CAAATAACTAATAC	500 nM, 10 min	GTATTAGTTATTTG TAGACGTAGG GTAATTGTTTTTAG	40 nM, 15 min

Figure S16A. OR-AND Cascade.

Logic Circuit	Input			Pre-dimerization	
	Name	Sequence	Condition	Sequence	Condition
OR-AND Cascade (X_1 OR X_2) AND X_3	X_1	CATTTTCTAAATAC ACAGCTAACA	500 nM, 15 min	GATTATAGATTATG TGGGATCTGT TGTTAGCTGT GTATTTAGAAAATG	10 nM, 15 min
	X_2	ACAGATCCCA CATAATCTATAATC	500 nM, 15 min		
	X_3	GAAATAGTTTATAG CTGCGACTGT GAATTTGTTATTAG	100 nM, 15 min	N/A	

Figure S16B. INHIBIT-AND Cascade

Logic Circuit	Input			Pre-dimerization	
	Name	Sequence	Condition	Sequence	Condition
INHIBIT-AND Cascade (X_4 AND NOT X_5) AND X_6	X_4	CTAAAAACAATTAC CCTACGTCTA CAAATAACTAATAC	200 nM, 15 min	GTATTAGTTATTTG TAGACGTAGG GTAATTGTTTTTAG	10 nM, 30 min
	X_5	GATTATAGATTATG TGTTAGCTGT GTATTTAGAAAATG	100 nM, 15 min	N/A	
	X_6	GAAATAGTTTATAG CTGCGACTGT GAATTTGTTATTAG	100 nM, 15 min		

Figure S17. OR-OR Cascade

Logic Circuit	Input			Pre-dimerization	
	Name	Sequence	Condition	Sequence	Condition
OR-OR Cascade (X_1 OR X_2) OR X_3	X_1	CATTTTCTAAATAC ACAGCTAACA	500 nM, 15 min	GATTATAGATTATG TGGGATCTGT TGTTAGCTGT GTATTTAGAAAATG	10 nM, 15 min
	X_2	ACAGATCCCA CATAATCTATAATC	500 nM, 15 min		
	X_3	CTATTACATAATTC TGCATTCTTC CATTATCATATAAC	500 nM, 15 min	GTTATATGATAATG GAAGAATGCA GAATTATGTAATAG	10 nM, 15 min

Movie S1. Time-lapse dark-field imaging of a nanoparticle Assembly YES gate.
A nanoparticle Assembly YES gate consists of a G-NF and a G-NF. In the presence of a DNA input (X_a in Fig. 1C) that forms a DNA bond at the receptor–floater interface via DNA hybridization (Input = "1"), a mobile G-NF binds to an immobile G-NR and forms a dimer. The assembly reaction results in an increase of green intensity of the G-NR scattering signal, which indicates a discrete switching of the G-NF from monomer state to dimer state (Output = "1"). G-NRs that generate outputs with G-NFs are marked with white circles before assembly and with yellow circles after assembly. The time-lapse video was recorded for 15 min after input addition. The input-induced assembly process is shown at the population level in the first part (0 s to 12 s). Real-time signal trace of a single-particle Assembly YES gate (chosen from the population-level imaging data) is shown in the second part (12 s to 24 s). Recording frame rate: 0.4 f.p.s. Playback at 30 f.p.s.

Movie S2. Time-lapse dark-field imaging of a nanoparticle Disassembly YES gate.
A nanoparticle Disassembly YES gate consists of a G-NR and a G-NF. Prior to input addition, G-NRs and G-NFs are assembled to form dimers by a single-stranded DNA strand (X_d* in Fig. 1C) that exposes a toehold domain (t_2 in Fig. 1C). The dimerization process was recorded by the dark-field time-lapse imaging at the population level for 15 min and is shown in the movie for the first 12 seconds. G-NRs that bind to G-NFs are indicated with white circles before assembly and with red circles after assembly. In the presence of a DNA input (X_d in Fig. 1C) that removes the preformed DNA bond X_d* via strand displacement (Input = "1"), the trapped G-NFs are released from G-NRs. The disassembly event results in a decrease of green intensity of the G-NR scattering signal, which indicates a discrete switching of the G-NF from dimer state to monomer state (Output = "1"). The released G-NFs are highly mobile. This disassembly process was recorded by the dark-field time-lapse imaging at the population level for the subsequent 15 min after input addition and is shown in the movie for the second part (12 s to 24 s). Real-time signal trace of a single-particle Disassembly YES gate (chosen from the population-level imaging data) is also shown in the third part of the movie (24 s to 36 s). Both pre-dimerization and disassembly processes were carried out in a fixed position. The G-NRs that release G-NFs are indicated with red circles before disassembly and gray circles after disassembly. Recording frame rate: 0.4 f.p.s. Playback at 30 f.p.s.

Movie S3. Receptor-only visualization of a dark-field movie.
A raw video (left) and the reconstructed video (right) with a small field-of-view (16 × 16 μm^2) time-lapse image are shown. The time-lapse imaging was conducted in high-speed (recording duration: 48 s; recording frame rate: 5 f.p.s.; playback at 30 f.p.s.) to image three mobile floater nanoparticles (R-NFs, G-NFs, B-NFs) and three immobile receptor nanoparticles (R-NRs, G-NRs, B-NRs) loaded with high density (~500 floaters and ~6,000 receptors in 128 × 128 μm^2). The receptor-only image sequence was generated based on the signals of receptor nanoparticles identified by the single-particle tracking algorithm described in fig. S6. No DNA inputs were added. Receptor signals are fluctuating, primarily due to the transient overlaps by mobile floaters bypassing in close proximity.

Movie S4. Time-lapse dark-field imaging of a two-input Assembly AND gate.
A two-input Assembly AND gate (X_1 AND X_2) consists of a G-NR (R_1 in Fig. 2A) and a G-NF (F_1 in Fig. 2A). Only when the two types of DNA inputs are both present in solution (1 AND 1), a mobile G-NF binds to an immobile G-NR and forms a dimer via DNA hybridization. The assembly reaction results in a step-function-like increase of green intensity of the G-NR scattering signal. Mobile G-NFs do not bind to G-NRs in other FALSE conditions (0 AND 0, 1 AND 0, 0 AND 1). G-NRs that assemble with G-NFs are indicated with white circles before assembly and with yellow circles after assembly. Each time-lapse video was recorded for 30 min after input addition. The raw videos are followed by reconstructed videos showing only G-NR signals. The first and last frames of the reconstructed movies are included in the second column of Fig. 2A. Recording frame rate: 0.4 f.p.s. Playback at 30 f.p.s.

Movie S5. Time-lapse dark-field imaging of a two-input Assembly OR gate.
A two-input Assembly OR gate (X_3 OR X_4) consists of a G-NR (R_2 in Fig. 2B) and a B-NF (F_2 in Fig. 2B). When either of two DNA inputs is present in solution (1 OR 0, 0 OR 1, 1 OR 1), a mobile B-NF binds to an immobile G-NR and forms a dimer via DNA hybridization. Mobile B-NFs do not bind to G-NRs in 0 OR 0 condition. G-NRs that assemble with B-NFs are indicated with white circles before assembly and with yellow circles after assembly. Each time-lapse video was recorded for 20 min after input addition. The raw videos are followed by reconstructed videos showing only G-NR signals. The first and last frames of the reconstructed movies are included in the second column of Fig. 2B. Recording frame rate: 0.4 f.p.s. Playback at 30 f.p.s.

Movie S6. Time-lapse dark-field imaging of a two-input Disassembly AND gate.
A two-input Disassembly AND gate (X_5 AND X_6) consists of a B-NR (R_3 in Fig. 2C) and a G-NF (F_3 in Fig. 2C). B-NRs and G-NFs are assembled to form dimers by two distinct DNA bonds (each exposing a unique toehold domain) in the pre-dimerization step prior to the input addition. Only when the two types of DNA inputs are both present in solution (1 AND 1), the two DNA bonds can be removed by strand displacement. The bond removal results in the release of G-NFs from B-NRs. The released G-NFs are highly mobile. The disassembly event does not occur in other FALSE conditions (0 AND 0, 1 AND 0, 0 AND 1). B-NRs that release G-NFs as outputs are indicated with red circles before disassembly and with gray circles after disassembly. Each time-lapse video was recorded for 15 min after input addition. The raw videos are followed by reconstructed videos showing only B-NR signals. The first and last frames of the reconstructed movies are included in the second column of Fig. 2C. Recording frame rate: 0.4 f.p.s. Playback at 30 f.p.s.

Movie S7. Time-lapse dark-field imaging of a two-input Disassembly OR gate.
A two-input Disassembly OR gate (X_7 OR X_8) consists of a B-NR (R_4 in Fig. 2D) and a B-NF (F_4 in Fig. 2D). B-NRs and B-NFs are assembled to form dimers by a DNA bond that exposes two distinct toehold domains in the pre-dimerization step prior to the input addition. When either of the two inputs is present in solution (1 OR 0, 0 OR 1, 1 OR 1), the DNA bond at the receptor–floater interface can be cleaved by strand displacement. The bond cleavage results in the release of B-NFs from B-NRs. The released B-NFs are highly mobile. The disassembly event does not occur in the condition 0 OR 0. B-NRs that release B-NFs as outputs are indicated with red circles before disassembly and with gray circles after disassembly. Each time-lapse video was recorded for 15 min after input addition. The raw videos are followed by reconstructed videos showing only B-NR signals. The first and last frames of the reconstructed movies are included in the second column of Fig. 2D. Recording frame rate: 0.4 f.p.s. Playback at 30 f.p.s.

Movie S8. Time-lapse dark-field imaging of a two-input Disassembly INHIBIT gate.
A two-input Disassembly INHIBIT gate (X_1 AND NOT X_2) consists of a G-NR (R_1 in Fig. 3A) and a G-NF (F_1 in Fig. 3A). G-NRs that release G-NFs as outputs are indicated with red circles before disassembly and with gray circles after disassembly. Each time-lapse video was recorded for 15 min after input addition. Recording frame rate: 0.4 f.p.s. Playback at 30 f.p.s.

Movie S9. Time-lapse dark-field imaging of a six-input Disassembly gate.
A circuit with an AND gate with fan-in from three OR gates [(X_3 OR X_4) AND (X_5 OR X_6) AND (X_7 OR X_8)] consists of a G-NR (R_2 in Fig. 3B) and G-NF (F_2 in Fig. 3B). G-NRs that release G-NFs as outputs are indicated with red circles before disassembly and with gray circles after disassembly. Each time-lapse video was recorded for 15 min after input addition. Recording frame rate: 0.4 f.p.s. Playback at 30 f.p.s.

Movie S10. Time-lapse dark-field imaging of a two-input Disassembly AND gate with three outputs.
A circuit with an AND gate (X_9 AND X_{10}) with fan-out to three YES gates consists of G-NR (R_3 in Fig. 3C), an R-NF (F_3 in Fig. 3C), a G-NF (F_4 in Fig. 3C), and a B-NF (F_5 in Fig. 3C). G-NRs that release floaters as outputs are

indicated with red circles before disassembly and with gray circles after disassembly. Each time-lapse video was recorded for 15 min after input addition. Recording frame rate: 0.4 f.p.s. Playback at 30 f.p.s.

Movie S11. Time-lapse dark-field imaging of a two-layer AND-AND cascade circuit.
A two-layer AND-AND cascade circuit [(X_1 AND X_2) AND X_3] consists of a G-NR (R_1 in Fig. 4B), a B-NR (R_2 in Fig. 4B), and a G-NF (F_1 in Fig. 4B). G-NRs that release G-NFs as outputs are indicated with red circles before disassembly and with gray circles after disassembly. B-NRs that generate the final outputs with the released G-NFs are indicated with white circles before assembly and with yellow circles after assembly. Each time-lapse video was recorded for 30 min after input addition. Recording frame rate: 0.4 f.p.s. Playback at 30 f.p.s.

Movie S12. Time-lapse dark-field imaging of a two-layer AND-OR cascade circuit.
A two-layer AND-OR cascade circuit [(X_4 AND X_5) OR X_6] consists of a B-NR (R_3 in Fig. 4C), a G-NR (R_4 in Fig. 4C), and G-NFs (F_2 and F_3 in Fig. 4C). Receptors that release G-NFs as outputs are indicated with red circles before disassembly and with gray circles after disassembly. Each time-lapse video was recorded for 15 min after input addition. Recording frame rate: 0.4 f.p.s. Playback at 30 f.p.s.

Movie S13. Time-lapse dark-field imaging of a nanoparticle multiplexer circuit.
A multiplexer circuit [(X_1 AND NOT *Sel*) OR (*Sel* AND X_2)] consists of G-NRs (R_1 and R_2 in Fig. 5) and G-NFs (F_1 and F_2 in Fig. 5). G-NRs that release G-NFs as outputs are indicated with red circles before disassembly and with gray circles after disassembly. Each time-lapse video was recorded for 15 min after input addition. The raw videos of the multiplexer responding to eight input combinations are followed by reconstructed videos showing only the signal response of receptors. Recording frame rate: 0.4 f.p.s. Playback at 20 f.p.s.